Aircraft Design Optimization Considering Network Demand and Future Aviation Fuels

Proesmans, P.; Morlupo, F.; Santos, Bruno F.; Vos, Roelof

DOI
10.2514/6.2023-4300

Publication date
2023

Document Version
Final published version

Published in
AIAA AVIATION 2023 Forum

AIAA AVIATION Forum
12-16 June 2023, San Diego, CA and Online
AIAA AVIATION 2023 Forum

10.2514/6.2023-4300

Aircraft Design Optimization Considering Network Demand and Future Aviation Fuels

P. Proesmans*, F. Morlupo†, B. F. Santos‡, and R. Vos§
Delft University of Technology, Kluyverweg 1 2629HS, Delft, The Netherlands

To reduce the climate impact of aviation, researchers are studying the replacement of fossil kerosene with liquid hydrogen and/or drop-in sustainable aviation fuel (SAF). These fuels can bring significant reductions in CO_2 emissions and can offer savings in terms of non-CO_2 climate effects. In addition, tube-and-wing aircraft can be optimized to decrease the global-warming impact by using a climate metric as a design objective rather than the operating costs. Previous research has shown that airplanes designed for minimal climate impact have a reduced cruise speed and fly at a lower altitude. This paper suggests a multidisciplinary, multi-level approach the evaluate the consequences of such design and fuels choices at the network level. Following the aircraft design step, a dynamic programming routine allocates the fleet and schedules the flights to maximize the network profit. We consider a hub-and-spoke network operating from Atlanta, with demand for domestic and international destinations. Compared to the reference cost-optimal kerosene fleet, a fleet consisting of climate-optimized kerosene aircraft can reduce the climate impact by 61% at a loss in network profit of approximately 21%. This design choice requires allocating an additional five aircraft. A fleet operating climate-optimal, hydrogen aircraft minimizes the climate impact. However, the high operating cost of long-range, hydrogen aircraft lowers the achievable profit. Aircraft powered by drop-in SAF provides Pareto-optimal solutions. These insights can be used to make decisions about the allocation of future aviation fuels in a network and the payload-range requirements of future aircraft.

Nomenclature

Latin Symbols

A	aspect ratio [-]
C_D	drag coefficient [-]
C	cost [USD per hour, km, or trip]
E_i	emission of species i [kg]
F	objective function
f_{PR}	payload-range envelope function
$\mathbf{g}$	constraint vector
h	altitude [m or ft]
k	aircraft type index [-]
M	Mach number [-]
m	mass [kg]
R	range [km]
S	wing area [m^2]
T	temperature [K] or thrust [N]
t	time [hours or years]
v	velocity [m/s]
W	weight [kN]
$\mathbf{x}$	aircraft design vector

Greek Symbols

ΔT	surface temperature change [K]
η_{ov}	overall propulsion efficiency [-]

Sub- and Superscripts

bl	block mission parameter
cr	cruise condition
eng	engine
f	flight index
L	lower bound
ref	reference scenario
U	upper bound

Acronyms

ATR	average temperature response
COC	cash operating cost
LR	long range
LHV	lower heating value of fuel [J/kg]
LTOT	landing and take-off time [hrs]
MTOM	maximum take-off mass [kg]

*PhD Candidate, Faculty of Aerospace Engineering, P.Proesmans@tudelft.nl, AIAA Student Member
†Researcher, Faculty of Aerospace Engineering
‡Associate Professor, Faculty of Aerospace Engineering
§Associate Professor, Faculty of Aerospace Engineering, AIAA Associate Fellow

OEM	operating empty mass [kg]
REG	regional
RPK	revenue passenger kilometer [km]
SMR	small, medium range
TAT	turn-around time [hrs]
TET	turbine entry temperature [K]
TLAR	top-level aircraft requirement
XDSM	extended design structure matrix

I. Introduction

REDUCING the climate impact of future aircraft is one of the top priorities in the commercial aviation industry at the moment. With a rising demand for air transport [1, 2], drastic changes in aircraft technology and operations are required to lower carbon dioxide (CO_2) emissions and reduce non-CO_2 effects. One way to reduce the impact of non-CO_2 effects, including the impact due to nitrogen oxide (NO_x) emissions and contrail formation, with current technology is to redesign the aircraft for a climate objective [3–6]. Such optimized aircraft fly at lower cruise altitudes to mitigate the radiative effects of ozone formation, contrails, and contrail cirrus. As a consequence of this low-altitude flight, the Mach number is reduced to remain at a near-optimal lift-to-drag ratio. However, this penalizes the mission block time and therefore the aircraft's productivity.

Combustion of novel fuels, such as liquid hydrogen or drop-in sustainable aviation fuels (SAF), can further reduce the climate impact by eliminating the CO_2 emissions in flight [7–9]. Additionally, the combustion of liquid hydrogen or SAF can also reduce the non-CO_2 climate effects. Since SAF has fewer soot particles than fossil kerosene and liquid hydrogen has none, it is expected that fewer ice crystals will be formed behind the engines, resulting in different contrail properties [10, 11]. A lower optical depth and a shorter lifetime can reduce the radiative forcing due to contrails. However, these fuels also increase the operating costs [12]. Additionally, the integration of hydrogen tanks into the aircraft adds to the empty operating mass (OEM) and increases the aircraft drag [13–15], which also leads to more energy consumption.

The introduction of slow-flying, climate-optimal, kerosene-powered aircraft will likely require a different allocation of the fleet. Additionally, replacing aircraft in the fleet with hydrogen- or SAF-powered alternatives may favor a different allocation and/or require different top-level aircraft requirements (TLARs). Therefore, a system-of-systems approach has to be taken to develop sustainable fleets where the aircraft and their operations are assessed simultaneously. Several research projects have implemented multi-level approaches. Jansen and Perez [16–18] proposed a method to optimize aircraft families and their allocation in different markets, showing that a reduction in fuel burn, operating and acquisition costs can be achieved. This requires solving optimizations at multiple levels, typically a nonlinear aircraft design optimization and a (mixed-integer) linear programming approach for fleet allocation. A similar approach was taken by Moolchandani et al. [19] to assess the environmental impact of new technologies, mainly focusing on CO_2 emissions. Hwang et al. [20] proposed a modular adjoint approach to solve such combined problems, resulting in fleet profit gains. Also, probabilities and uncertainties in aircraft technologies and forecasts can be taken into account [21]. Govindaraju et al. [22] employed a multi-level approach to study potential fuel burn savings under operational uncertainty.

Although the problem of coupled aircraft design and fleet allocation has been studied in the literature, the challenge of increased block time of climate-optimal aircraft and the effect on aircraft design and fleet allocation has not yet been examined in detail. In addition, we would like to know how fuel selection plays a role in this and how to allocate novel fuels optimally.

Therefore, this paper proposes a multidisciplinary, multi-level approach to address these two issues. The first research question we address is: considering an available network demand, what is the optimal fleet diversity and allocation of climate-minimal, kerosene aircraft in an airline network to maximize the profit? Once we have gained insight into how these aircraft should be redesigned and allocated, we can extend the problem to examine how future aviation fuels can further reduce the climate impact of the network. We will monitor the effects on total network profits and energy consumption in this extended problem.

To answer these research questions and gain insight into the fleet-level impact of redesigned aircraft and multiple fuels, we make use of a conceptual, multidisciplinary aircraft design framework and dynamic programming fleet allocation model. A linearized temperature response model analyzes the climate impact of the fleet in terms of the average temperature response (ATR_{100}), which considers both CO_2 and non-CO_2 effects [4]. Note that this multi-level problem considers a fixed weekly network demand and that we do not consider changes in demand or fleet composition with time in the current study. Additionally, it is possible that network and airline markets may change depending on the available aircraft in the future, while we assume the network demand to be the driving factor for new aircraft in this study.

This paper is structured as follows. In Section II, we introduce the approach to design and allocate aircraft. Subsequently, we construct a cost-optimal reference case that only employs kerosene-powered aircraft in Section III. By studying this reference case, we can verify the coupling between the two levels and evaluate the decision-making process of the dynamic programming routine. In Section IV, we address the two research questions introduced above. Finally, the method and results are summarized in Section V.

II. Multidisciplinary Setup and Methods

To address the research question formulated above, we propose to extend a multidisciplinary aircraft design and optimization framework with a second level to perform fleet allocation and flight scheduling. This setup is employed to design aircraft of different sizes, burning different fuels, and allocate these aircraft optimally on a chosen network. First, we further clarify the overall problem of interest and the setup in Section II.A. Subsequently, Sections II.B and II.C focus on the two levels, namely aircraft design and fleet allocation, respectively. The methods to evaluate the network cost and climate impact are treated in Sections II.D and II.E

A. Multidisciplinary Problem Definition and Setup

The multidisciplinary design analysis and optimization (MDAO) setup tries to solve two problems: first, the optimization of aircraft for given top-level aircraft requirements (TLARs) and selected objective functions. The aircraft design objective functions considered in this study are the cash operating costs (COC) and the climate impact quantified by the average temperature response over a period of 100 years (ATR_{100}). This aircraft design optimization is done for three sets of top-level aircraft requirements corresponding to different market segments (regional, medium-, and long-range). The second goal of the MDAO framework is to consider this set of aircraft types, designed for the same objective, and to allocate them on a given route network to maximize the profit on that network.

By taking this two-step approach, we can analyze how the aircraft types designed for a single objective function are used together in a fleet, the overall achievable profit over a network, and the climate impact of the scheduled operations. In particular, we can study how the fleet composition and schedule change with varying aircraft design objectives. The aircraft design step can also design aircraft with the same top-level requirements and objectives but with different fuels, such as drop-in sustainable aviation fuels (SAF) or liquid hydrogen. Hence, this setup allows assessing how the aircraft designed for different objectives and fuels drive the fleet composition and schedule.

Figure 1 presents the overall strategy and workflow. Block 0 in this diagram manages the aircraft design optimization defined in Equation (1). The first level (steps 1 to 6) is the aircraft design loop which ensures that consistent and feasible aircraft are created. The details of the aircraft design process are discussed in Section II.B. The aircraft design routine passes on flight performance information, such as the drag polar and engine deck parameters, for fleet allocation and fleet-level assessment of energy consumption, climate impact, and profit. This aircraft design loop covers three sets of top-level requirements, covering three market segments. This multi-aircraft analysis is highlighted by the stacked disciplines in Figure 1, in comparison to the network-level analysis considering all three aircraft simultaneously. The information of all three aircraft is passed on to the second level since all three aircraft types are considered for allocation simultaneously.

The second level (steps 7 to 11) allocates the synthesized aircraft on the network to maximize the profit, considering the available network demands between origin-destination pairs, which are for example imposed by an airline. The demand and airports to be included are gathered in the "Network Info" block in the top row of the XDSM. This information is fixed for all considered cases. Section II.C elaborates upon the steps in the fleet allocation model. Once an optimal allocation and schedule are created, the climate impact of this network is evaluated.

By running this workflow for different aircraft design objectives and fuels, the resulting schedules can be compared regarding profit and climate impact. Additionally, since the allocation of passengers is an output of the fleet allocation, updates to the initial top-level aircraft requirements, such as maximum structural payload mass and design range, can be proposed, which are tailored to the design objective and/or fuel. However, the automated update of such top-level parameters is considered outside the scope of this paper and is proposed as a recommendation.

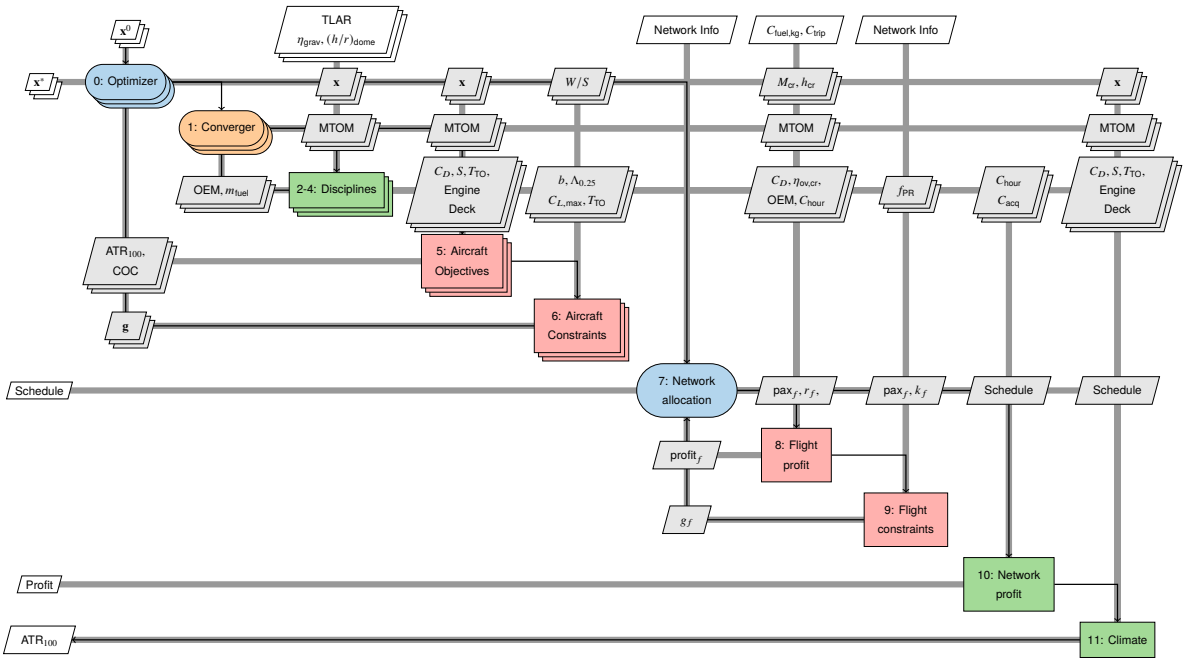

Fig. 1 Extended design structure matrix (XDSM) representing the multidisciplinary workflow

B. Aircraft Design Optimization

The aircraft design optimization is similar to the setup in previous research [6, 12]. This section provides a summary of this multidisciplinary aircraft design framework. The optimization considers two objective functions, the cash operating costs, and the climate impact, and controls the aircraft design by nine aircraft design variables targeting the airframe, turbofan engines, and mission profile. The optimization problem, independent of top-level requirements and fuel choice, is formulated as follows:

$$\begin{aligned} \underset{\mathbf{x}}{\text{minimize}} \quad & F(\mathbf{x}) = \text{ATR}_{100}(\mathbf{x}) \quad \text{or} \quad \text{COC}(\mathbf{x}) \\ \text{subject to} \quad & x_i^L \leq x_i \leq x_i^U \quad \text{for } i = 1, 2, ..., 9, \\ & g_j \leq 0 \qquad\quad \text{for } j = 1, 2, ..., 5 \end{aligned} \tag{1}$$

where x_i are the nine design variables, collected in vector $\mathbf{x}$, and g_j are five inequality constraints. The aircraft design variables for the aircraft under consideration are presented in Tables 4, 16 and 17. The inequality constraints g_j impose limits on the wing loading, wing span, lift cruise coefficient, and engine technology parameters such as turbine entry temperature at take-off (TET) and maximum overall pressure ratio (OPR).

The aircraft design process is based on conceptual methods considering several disciplines. The setup of the workflow is similar for all aircraft categories and fuel types, although different input values are used. The workflow employed in this study is based on existing methods discussed in References [6] and [12]. The disciplinary analyses (block 2-4 in Figure 1) are run sequentially until the maximum take-off mass (MTOM) and operating empty mass (OEM) of the aircraft converge. Three main disciplines are collected in the disciplines block 2-4 in Figure 1, namely the airframe design, propulsion, and mission analysis. The following paragraphs summarize the inputs, outputs, and working principles of these disciplines.

Airframe Design The airframe design discipline includes four steps being the Class-I sizing, the geometry creation, the aerodynamic analysis, and the Class-II mass estimation. These disciplines use the design variables selected by the optimizer and the current MTOM estimate to conceptually size the fuselage, wing, and empennage, and assess aerodynamic and structural properties required in subsequent disciplines. The size and mass of the engines are determined separately in the propulsion module.

The Class-I sizing module uses the MTOM to determine the wing area and take-off thrust of the aircraft. These two parameters are derived from the wing loading W/S and thrust-to-weight ratio T/W. The wing loading is a

design variable, while the module selects the thrust-to-weight ratio automatically so that performance and regulatory requirements are met. These requirements are related to the take-off distance, cruise speed and cruise altitude, and climb gradients in one-engine-inoperative and balked-landing conditions.

All aircraft considered in this study have a tube-and-wing configuration with two turbofan engines mounted on the wing. Based on the wing area and payload requirements, a conceptual geometry of the aircraft is generated according to the design rules discussed in Appendix C of Reference [6]. The wing is sized according to the chosen wing loading and the estimated MTOM of the aircraft. The discipline automatically updates the wing planform according to the selected aspect ratio and cruise Mach number, which drives the wing sweep and taper ratio.

The fuselage cabin is sized according to a one-class layout, with four, six, and nine seats abreast for regional, medium- and long-range aircraft, respectively. For hydrogen-powered aircraft, a liquid hydrogen tank is positioned aft of the cabin in the fuselage. This tank is cylindrical with ellipsoidal end caps, fitted to the inner diameter of the fuselage. The length is subsequently derived from this diameter and the total required volume. This volume follows from the maximum fuel mass required and the density of liquid hydrogen (approximately 71 kg/m^3). This tank elongates the fuselage tail section increasing the fuselage structural mass and zero-lift drag component. This is reflected in the following aerodynamic and mass disciplines.

The next step in the airframe design chain is to estimate the drag polar of the aircraft, abbreviated by C_D in Figure 1. We assume the drag polar to be quadratic, with a zero-lift drag term and a lift-dependent drag term. The first term is computed by adding the contributions of individual aircraft components [6, 23]. The lift-induced component of the quadratic polar scales with the effective aspect ratio of the wing and the Oswald factor, which is determined statistically as a function of the chosen wing aspect ratio [23]. To account for drag-reducing wing tip devices, 5% is added to the geometric aspect ratio to obtain the effective aspect ratio, which is used in the drag polar throughout the MDAO chain.

The final step in the airframe design is to assess the operating empty mass of the aircraft based on the geometry and expected loads. We use the methods from Torenbeek [24] to analytically estimate the masses of component groups such as the fuselage, wing, empennage, and undercarriage. The masses of operational items and fixed airframe systems and equipment are set for each aircraft category and thus do not change with fuel. The assumed values are included in Table 15. For the cryogenic hydrogen tank, a fixed gravimetric index η_{grav} of 0.4 is assumed, which relates the tank mass to the maximum fuel mass it can hold [12].

Propulsion All aircraft are powered by two turbofan engines mounted onto the wings. The propulsion model determines the performance of these engines with physics-based, 1D thermodynamic on- and off-design models [25], considering a variable-specific heat model [26]. The engine cycle is determined and the engine is sized according to the required thrust levels in cruise and take-off. The performance output of this module consists of fuel and energy consumption, as well as the emissions of various species, including CO_2, NO_x, soot, and sulfate (SO_4). The 1D thermodynamic model is required to compute the temperature and pressure at the combustor inlet and calculate the emission index of NO_x.

The engine performance depends on the exhaust gas composition, which varies between the different fuels. Therefore, two gas models are implemented: one for fossil kerosene and SAF [26], and one for the combusted hydrogen mixture, which contains more water vapor than the other two fuels but no carbon-based molecules [27]. Several types and production pathways exist for drop-in SAF. In this paper, we assumed a 50-50 mixture of traditional kerosene with hydro-processed esters and fatty acids (HEFA). Furthermore, the calorific values and emission indices are different for each of the fuels. Table 1 summarizes the values used per fuel type.

Table 1 Overview of calorific values and emission indices for fuel types under consideration [4, 12]

	Kerosene	**SAF 50%**	**Hydrogen**
LHV [MJ/kg]	43.0	43.6	120
EI CO_2 [kg_{CO_2}/kg_{fuel}]	3.16	1.58	0.
EI H_2O [kg_{H_2O}/kg_{fuel}]	1.26	1.32	8.93
EI Soot [kg_{Soot}/kg_{fuel}]	4.0×10^{-5}	2.0×10^{-5}	0.
EI SO_4 [kg_{SO_4}/kg_{fuel}]	2.0×10^{-4}	1.0×10^{-4}	0.

Mission Based on the aircraft mass, aerodynamic characteristics, and engine performance obtained in the previous disciplines, the mission module updates the mission fuel mass required. Together with OEM estimation from the Class-II mass calculation and the payload mass, this fuel mass allows the converger to update the MTOM of the aircraft. The mission module computes the mission fuel according to the methods laid out by Torenbeek [28]. These methods are largely independent of the fuel type (kerosene, SAF, or liquid hydrogen) except for the statistical coefficients used for the maneuvering, diversion, and loiter phases. Therefore, the methods are augmented for hydrogen with the Breguet equations for diversion and loiter [29].

C. Fleet Allocation

Steps 7 to 11 of Figure 1 allocate the aircraft designed in steps 1 to 4 on a given network to maximize the profit while considering operational constraints. The network profit is defined as the sum of all profits collected over all allocated flights minus the ownership costs of all assigned aircraft. The dynamic programming method was chosen to model the fleet assignment problem. Dynamic programming is an optimization method that breaks down a complex problem into smaller, simpler sub-problems and solves each sub-problem only once, storing the solution to avoid redundant calculations. This approach allows for efficient solutions to otherwise computationally infeasible problems. Dynamic programming has been widely used in aviation to optimize operational problems. The methodology adopted in this study was inspired by the work of Seaone Álvarez [30] and Noorafza et al. [31]. Figure 2 shows how the algorithm works.

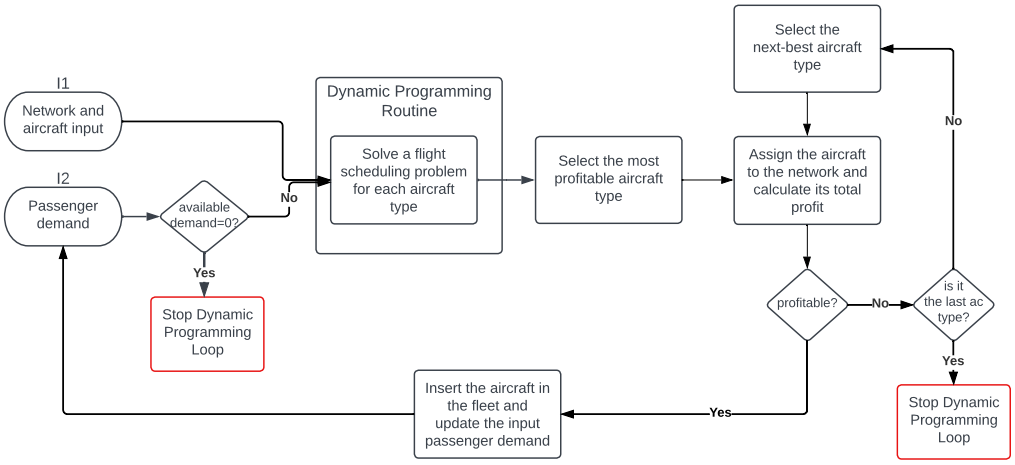

Fig. 2 Dynamic programming approach employed to solve the fleet allocation problem (adapted from [30])

The approach requires two distinct types of input data, which are labeled with different numbers. In block I1, there is all the network-related information, such as the network type, operated routes, airport data, and fleet-related data, such as aircraft types, seating capacity, range, and fuel consumption. More information on this input data can be found in Section III.A. Block I2 consists of passenger demand data, which is elaborated upon later in this section. This block is subject to a condition that must be verified before initiating the dynamic programming routine: passenger demand must exist (or must be greater than a certain value chosen by the airlines).

Once the passenger demand condition is verified, the dynamic programming routine is initiated. Within this block, a flight scheduling problem is solved for each aircraft type in the fleet, with the objective of identifying the aircraft type that yields the highest operational profit. The most profitable aircraft is then virtually assigned to the network, its flight schedule is built, and its overall profit is determined, including the aircraft ownership costs. If the total profit is greater than zero (or greater than a benchmark chosen by the airline), the aircraft is added to the fleet. Otherwise, the procedure is repeated for the next-best aircraft type, and so on until a profitable aircraft type is found.

If none of the aircraft types are profitable or no demand is left, the algorithm stops. However, if a profitable aircraft type is identified, the aircraft is added to the fleet, and the passenger demand assigned to its schedule is removed from the input data. The cycle repeats iteratively until one of the two stopping criteria is met. Ultimately, the algorithm output is the best aircraft fleet for the airline (i.e., how many aircraft instances of each aircraft type), along with the weekly schedule for each aircraft.

Flight Scheduling Problem The idea behind dynamic programming is the possibility of solving one sub-problem at a time. Each time the dynamic programming routine is accessed, as many sub-problems are solved as there are aircraft types available. Each sub-problem is a flight scheduling problem with only one aircraft and it is solved using the Bellman-Ford algorithm [32, 33]. The Bellman-Ford algorithm is a shortest path algorithm that can be used to find the shortest path between two nodes in a graph. In this case, the graph is built on a space-time network, where the spatial coordinates are the airports and the temporal coordinates are the time bands (whose width is the resolution of the model). The algorithm works by repeatedly relaxing all edges in the graph until the shortest path distances converge. In this study, it is used to find the best route for each aircraft with the goal of maximizing operational profit. The output consists of the best schedule for the aircraft under consideration. The problem is subject to the following three operational constraints:

1) the number of passengers carried and the distance to be flown must fall within the aircraft's range-payload diagram. The payload-range envelope is modeled as a function (f_{PR} in Figure 1) which returns the maximum allowed payload mass for a certain aircraft type at a certain range;
2) a flight cannot depart after the airport closure for curfew and cannot land before the airport opening at the end of curfew;
3) a flight cannot depart if the departure airport's runway is shorter than the aircraft's required runway or if the arrival airport's runway is shorter than the aircraft's required runway.

This dynamic programming approach offers increased flexibility and reduces computational time compared to exact optimization methods, but provides a sub-optimal solution. However, the optimality of the resulting schedule is not the primary focus of this research and does not affect the validity of the results obtained. These results mainly focus on the differences in the allocation of fleets with aircraft fueled by different fuels or designed for different objectives.

Demand Input Modeling and Passenger Selection In this problem formulation, we are considering the period of one week. Therefore, the passenger demand per origin-destination (OD) pair is an input to the model. Nevertheless, the demand throughout the week is not constant. The required input is a demand schedule per OD pair where the weekly demand is divided into discrete demand peaks throughout the peak, around which the demand is normally distributed. For each OD pair, this results in an array of 504 elements of 20-minute intervals. Each interval has either no demand (0) or a positive integer indicating the number of passengers willing to travel a specific route at that time. This approach ensures that it will be more attractive to keep flying at certain high-demand periods, no matter what the design objective of the aircraft is. Hence, we can assume that in general passenger preferences will still be regarded when defining the flight schedules and that the airline remains competitive. Visual representations of such demand schedules are provided in Figures 3 and 8a.

This demand schedule influences how many passengers can be transported between an origin-destination pair at the departure time under consideration by the algorithm. As discussed above, the input to the allocation problem is a demanding schedule where each demand peak is spread out over multiple time slots of 20 minutes. When the algorithm considers a possible flight at a given departure time slot, the maximum passenger number that can be taken on board is the minimum value of either

- the demand available in that 20-minute time slot plus the demand available in the surrounding n_{attr} time slots, or
- the maximum amount of seats the aircraft type under consideration, multiplied by a given load factor.

The parameter n_{attr} is the attraction band. In the current study, the attraction band is set to nine, meaning that the algorithm can pick up any available demand from the three hours prior and three hours after the considered departure time. This simulates the willingness of a subset of the passengers to take a slightly earlier or later flight. This passenger selection at a departure time t for route i can be formulated as follows:

$$\mathrm{pax}_{i,t} = \min\left(\mathrm{seat}_k \cdot \mathrm{LF}_k \,,\ \sum_{x=t-n_{\mathrm{attr}}}^{t+n_{\mathrm{attr}}} \mathrm{demand}_{i,x}\right) \tag{2}$$

Model Considerations The approach presented and adopted in this research is based on some model considerations, both methodological and numerical. The most significant considerations are listed below:

- The objective is to maximize profit. Also when aircraft which are optimized for a climate objective are used, we assume that the operator would still prefer to maximize its profits;
- The model simulates an average week of operations, thus it produces the flight schedules for 7 days;

- Time resolution of the model is 20 minutes. The resolution of the model indicates the width of the time intervals in which time is discretized. This concept is used to represent the airline flight network on which the Bellman-Ford algorithm is applied.

Furthermore, when developing the schedule for a particular aircraft, the algorithm considers a turn-around time (TAT) between two consecutive flights. We consider this turn-around time to be particular to a certain aircraft type and independent of the number of passengers onboard. The turn-around time (in hours) is approximated using the relation proposed by Perez and Jansen [18]:

$$\mathrm{TAT}_k = \left(2.0 + \frac{n_{\mathrm{seats},k}}{c_1 \cdot n_{\mathrm{doors},k}} + \frac{n_{\mathrm{seats},k}}{c_2} + \frac{n_{\mathrm{seats}}}{c_3 \cdot n_{\mathrm{doors},k}} + 3.0\right) / \ 60 \tag{3}$$

where $n_{\mathrm{seats},k}$ and $n_{\mathrm{doors},k}$ are the number of seats and opened doors for aircraft type k, respectively. In practice, the TAT may vary depending on how many passengers are carried on board a specific flight. However, in this study, we assume a constant, conservative turn-around time with the maximum number of seats occupied and only one open door at the gate for all flights.

D. Operating Cost Analysis

In the dynamic programming routine, the operating costs for each potential flight have to be calculated to assess the achievable operational profit. In this study, we only consider the direct operating costs (DOC), which are mostly driven by the aircraft design, and neglect the indirect operating costs which are strongly dependent on airline strategic decisions. The direct operating costs are dependent on fuel consumption, oil usage, crew costs, maintenance costs, insurance, and landing fees. The cost to execute a flight, C_f, is defined as follows:

$$C_f = C_{\mathrm{fuel}} + C_{\mathrm{oil}} + C_{\mathrm{crew}} + C_{\mathrm{maint}} + C_{\mathrm{ins}} + C_{\mathrm{landing}} \tag{4}$$

$$= C_{\mathrm{fuel/kg}} \cdot m_{\mathrm{fuel,bl}} + C_{\mathrm{hour}} \cdot t_{\mathrm{bl}} + C_{\mathrm{landing}} \tag{5}$$

The fuel costs are calculated from the fuel mass consumed on that particular flight. This fuel mass is estimated using the analytic relations from Torenbeek's lost-range method [28] where the cruise range is set to the great circle distance between the origin and destination of the considered flight. The payload mass is dependent on the number of passengers assigned to this flight by the allocation algorithm. The lost-range method also includes fuel spent during take-off and climb as a function of the initial cruise altitude and velocity and adds a fraction to account for maneuvering. Additionally, reserve mission fuel is considered in the mass estimation, but this part is not added to the cost estimation since it is unlikely that this fuel is used on every flight.

The landing fee C_{landing} is a fixed fee per flight. In the current model, this fee is assumed to be the same for every airport in the network. We assume that the other cost elements in Equation (5) scale with the block time t_{bl} of the flight. The block time is the sum of four terms: 1) the cruise time, 2) the time spent in take-off, climb, descent, and landing, 3) the time covered by ground maneuvers such as taxiing to and from the runway, and 4) the time covered in the air for maneuvering. The cruise time is equal to the great circle distance between the origin and destination divided by the cruise speed. We estimate the flight time before and after cruise by performing a numeric mission of the aircraft. We determine the ground maneuvering time t_{gm} the relation suggested by Roskam [34]:

$$t_{\mathrm{gm}} = 0.51 \cdot 10^{-6} \cdot \mathrm{MTOM} + 0.125 \tag{6}$$

where MTOM is the aircraft's maximum take-off mass in kilograms. Ten minutes are added to account for airborne maneuvers. All non-cruise time components are collected in the landing and take-off time parameter (LTOT). This time is also taken into account in the scheduling algorithm. The time spent on ground operations while the aircraft is parked, such as the unloading and loading of passengers, is not added to the block time but is considered in the turn-around time between flights, as discussed above. This time-dependent cost term C_{hour} is based on the methods introduced by Roskam [34] and uses cost estimates from 2022 [12].

As discussed in the fleet allocation algorithm section, once the most profitable aircraft is selected, the net profit has to be computed by subtracting the weekly ownership costs from the profits obtained from the flights throughout the week. This ownership cost is modeled as an annual fee for acquiring the aircraft, either through purchase or leasing. The annual leasing cost is assumed as a fraction of the aircraft purchasing price [17]:

$$C_{\mathrm{acq,week},k} = 0.0835 \cdot \mathrm{APP}_k / 52 = 0.0835 \cdot \left(\mathrm{AFP}_k + n_{\mathrm{eng}} \cdot \mathrm{EPP}_k\right) / \ 52 \tag{7}$$

where AFP is the airframe purchase price and EPP is the engine purchase price. These prices are estimated from relations based on aircraft operating empty mass and engine take-off thrust, respectively [35]. The daily ownership cost for aircraft type k is equal to $C_{\text{acq,week},k}$ divided by seven in the current setup. This approach may underestimate the daily or weekly ownership costs since an aircraft does not operate every day because of maintenance tasks, for example.

E. Climate Impact Assessment

Once the fleet has been allocated and the schedule is known, the climate impact of the network can be evaluated. The climate impact cannot be calculated during the fleet allocation iterations since the computation is nonlinear and requires a multi-year emission scenario as input which is not known when the objective function is evaluated due to the backward-solving procedure of the dynamic programming routine. An alternative approach would be to consider the emission and contrail length during the schedule creation as metrics for climate impact. However, this would not capture differences in the short- versus long-term effects of the different species. In this research, the climate impact is measured by the average temperature response over a period of 100 years (ATR_{100}). This metric is defined as the averaged integral of the temperature response ΔT over a period H:

$$\text{ATR}_H = \frac{1}{H} \int_0^H \Delta T(t)\, dt \tag{8}$$

where the unit of variable t is one year. The temperature response is calculated using a linearized temperature response model [4, 12]. This parameter considers the effects due to carbon dioxide (CO_2) emissions, nitrogen oxides (NO_x) emissions, contrail formation, and emissions of soot and sulfate (SO_4). While the effects of NO_x and contrails on $\Delta T(t)$ are typically short-lived (from hours to decades), the warming effect due to CO_2 emissions can span over centuries. Therefore, we select a period of 100 years which provides a balance between the short- and long-lived effects [36].

The time horizon under consideration starts in 2023 and continues until 2123. We assume that the fleet operates for 35 years, approximately the lifespan of an aircraft, and that the network schedule is repeated 52 times per year. This leads to an operational scenario where the annual emissions and contrail formation are constant, but non-zero, for the first 35 years and then abruptly fall to zero from 2058 onward. In reality, it is likely that network demand will increase in the future [1, 2] and that the fleet composition will change due to this growth, new technologies, and potential policies. This growth effect is not captured in the approach since we assume a steady demand. However, this approach allows us to answer the research questions posed in Section I which focus on the comparison of fleets and aircraft designs, rather than accurately computing the actual climate impact of a future scenario.

To create the 35-year emission scenario, the emissions for all flights in the weekly schedule have to be computed and added. The carbon dioxide emissions follow directly from fuel consumption. However, the NO_x emissions and contrail formation have to be evaluated at discrete steps in the mission since these effects are altitude dependent. Therefore, a numeric mission analysis is carried out for each unique flight performed in the weekly schedule. A unique flight is defined by the route, the aircraft type, and the number of passengers carried, since this will affect the flight performance.

The data per flight obtained through this mission analysis are the CO_2 emissions, NO_x emission distribution per flight level, and contrail length distribution per flight level. For each of these climate species, these values and distributions are multiplied by the frequency of this particular flight and subsequently added to achieve the total value or distributions of the one-week period. Finally, the data is multiplied by 52 to model the contribution of one year. The emission indices, contrail formation criteria, and contrail properties are different for each considered fuel. In this study, we assume the data collected in Table 1.

The linearized temperature response model [4, 6] first translates the emission scenario into radiative forcing, then normalized radiative forcing, and finally into the temperature response. This model considers the warming effects due to changes in atmospheric concentrations due CO_2, short-term ozone (as a result of NO_x emissions at altitude), as well as the warming effects due to contrails. The effect of contrails is currently studied and may consist of warming and cooling effects [37], depending on the time and location. However, in this study, we assume that the net effect results in global warming. The temperature response calculations also consider the cooling effects due to long-term methane and ozone depletion as a result of NO_x emissions.

III. Cost-Optimal Reference Case and Verification

This section introduces the reference network on which the different aircraft sets will be allocated. In this section, we focus on the allocation of cost-optimal, kerosene aircraft, which allows us to verify the dynamic programming approach and provides a reference case for the solutions in Section IV. The aircraft design methods have been verified in earlier research for the three aircraft categories [6, 12], but the connection to the network level is new in this paper. Therefore, the verification step here targets the connection between the aircraft design, the fleet allocation, and the fleet allocation model itself. Note that the fleet allocation algorithm requires inputs and assumptions, such as airport landing fees and ownership costs, which are not made publicly available for all airports or operators. Therefore, the verification in this section aims at reproducing the realistic decision-making of an operator rather than obtaining 100% accurate cost or profit measures.

A. Reference Network Demand Data and Cost-Optimized Aircraft

The reference network we consider is based upon the North American network operated by Delta Airlines, as introduced by Jansen and Perez [38]. The hub of this network is Atlanta Airport (ATL). From this hub, we consider passenger demand towards nineteen domestic and eleven international airports. The passenger demand introduced in the work by Jansen and Perez is translated into a weekly demand and gathered in Table 2. The demand for the five additional transatlantic routes is taken from the Bureau of Transport Statistics (BTS) Air Carriers: T-100 International Segment (US Carriers Only) * database. We assume that the network demand in Table 2 is symmetric, meaning that there is an equal weekly demand from each destination airport to Atlanta.

The weekly passenger demand is transformed into a demand schedule, as introduced in Section II.C. This proposed schedule assumes demand peaks at discrete times throughout the week. The demand at a particular time is subsequently distributed over a three-hour interval, with the peak time at the center of the interval. If an aircraft cannot depart at the time of the peak due to surrounding flights, for example, it can still capture a fraction of the demand because of this distribution. We assume that for each demand peak, a six-hour window exists in which passengers are willing to depart.

Figure 3 shows examples of the demand schedules for the Atlanta-Boston and Atlanta-Amsterdam connections. The demand schedule for domestic routes is set up such that multiple demand peaks are present each day, representing an expected daily frequency of 6 or 7. For transatlantic routes, the demand is modeled after the current flight departure times in the late afternoon or early morning. The heatmap in Figure 8a shows how the demand for each route in the network is spread throughout the week, per time step of 20 minutes, for the considered network. The dark green regions indicate the highest demand, while the light yellow regions indicate moments of zero demand. The demand schedule is arranged so that each route's highest demand occurs during the day. For each airport, departures have to occur between five o'clock in the morning and eleven in the evening, representing a curfew of six hours each day.

Since the objective of the fleet allocation is to maximize the network's profit, the allocation needs cost and yield estimates as input. Table 3 provides an overview of the assumptions for the reference network. The remaining overnight parking cost applies whenever an aircraft has to spend the night at an airport other than the hub, which is Atlanta Airport. Because of airport curfews, sometimes the aircraft cannot return to the hub on the same day and has to be parked at the destination airport. Typically, this period is less than eight hours long. A landing fee is added to the operating costs for each flight. The remaining overnight and landing fees are assumed to be the same for all considered airports, although, in practice, these numbers will be different for each airport or country. The yield per passenger-kilometer in Table 3 is an average value based on economy-class ticket prices over the considered routes in 2023 †.

The baseline set of aircraft consists of three aircraft types which are all optimized to minimize the cash operations costs at the aircraft level. Table 15 summarizes the top-level of these three aircraft categories, targeting the regional, medium-, and long-range market segments. In the upcoming sections, these three aircraft types are referred to using the acronyms "REG", "SMR", and "LR". The top-level requirements are based on existing aircraft [40–42], and these requirements are the same for all considered aircraft design objectives and fuels in this research.

The design variables and performance data for the kerosene-powered aircraft types are presented in Table 4. The chosen design variables result from the optimization defined in Equation (1) and are based on the work performed in previous research [12]. We use the data of the aircraft designed for the minimal operating cost (COC columns in Table 4) to define the reference scenario and to complete the verification step in Section III.B. The provided mass and performance metrics are inputs to the fleet allocation model.

*URL `https://www.transtats.bts.gov/Fields.asp?gnoyr_VQ=GDK` accessed on 19 April 20223

†URL `https://www.delta.com/flight-search/book-a-flight` accessed on 19 April 2023

‡URL `https://www.iata.org/en/publications/economics/fuel-monitor/` accessed on 2 April 2023

Table 2 Reference network weekly passenger demand data

Origin Airport	Destination Airport	Destination Country	Demand
Atlanta (ATL)	Los Angeles (LAX)	USA	6442
Atlanta (ATL)	Minneapolis (MSP)	USA	5849
Atlanta (ATL)	Boston (BOS)	USA	5280
Atlanta (ATL)	Dallas-Fort Worth (DFW)	USA	4908
Atlanta (ATL)	Miami (MIA)	USA	4760
Atlanta (ATL)	Salt Lake City (SLC)	USA	4611
Atlanta (ATL)	San Francisco (SFO)	USA	4212
Atlanta (ATL)	New Orleans (MSY)	USA	4193
Atlanta (ATL)	Detroit (DTW)	USA	3932
Atlanta (ATL)	Denver (DEN)	USA	3658
Atlanta (ATL)	Seattle (SEA)	USA	3528
Atlanta (ATL)	Paris (CDG)	France	3438
Atlanta (ATL)	Phoenix (PHX)	USA	3406
Atlanta (ATL)	London (LHR)	UK	2896
Atlanta (ATL)	Columbus (CMH)	USA	2508
Atlanta (ATL)	Savannah (SAV)	USA	2273
Atlanta (ATL)	Cancun (CUN)	Mexico	2136
Atlanta (ATL)	Dublin (DUB)	Ireland	2084
Atlanta (ATL)	Buffalo (BUF)	USA	1943
Atlanta (ATL)	Amsterdam (AMS)	The Netherlands	1860
Atlanta (ATL)	Rome (FCO)	Italy	1689
Atlanta (ATL)	Portland (PDX)	USA	1577
Atlanta (ATL)	Albuquerque (ABQ)	USA	1327
Atlanta (ATL)	Munich (MUC)	Germany	1289
Atlanta (ATL)	Tucson (TUS)	USA	984
Atlanta (ATL)	Manchester NH (MHT)	USA	625
Atlanta (ATL)	Guadalajara (GDL)	Mexico	589
Atlanta (ATL)	Caracas (CCS)	Venezuela	455
Atlanta (ATL)	Georgetown (GCM)	Cayman Islands	422
Atlanta (ATL)	Quito (UIO)	Ecuador	392

B. Verification

By performing the allocation routine for the network and the three cost-optimal, kerosene aircraft introduced in the previous section, we find that the profit is maximized by allocating 36 aircraft. This fleet consists of eight regional aircraft, 21 medium-range aircraft, and seven long-range aircraft. The total network profit in one week is approximately 23.4 million USD, including operating and ownership costs according to Section II.D. However, this figure does not include any indirect operating costs or taxes related to emissions or noise. The profit margin for these aircraft on this network is approximately 3.4%.

Figure 4 shows the convergence of the network profit and transported revenue passenger versus the aircraft added to the operational fleet. The aircraft added correspond to the iterations carried out by the allocation algorithm (see Figure 2). As can be seen in Figure 4, first large passenger aircraft are added, which offer large profits on long-range, intercontinental flights. The corresponding routes are shown in Figure 5c. However, the long-range aircraft do not cover the most RPKs, as can be seen from the distribution in Table 5. Subsequently, small, medium-range aircraft

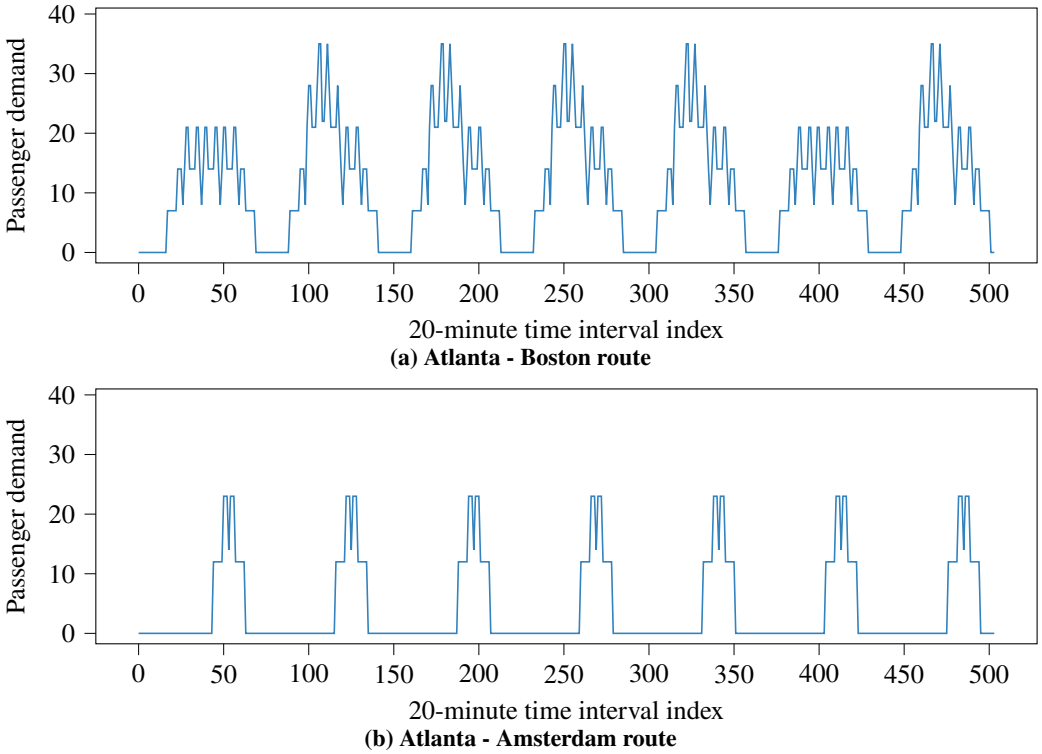

(a) Atlanta - Boston route

(b) Atlanta - Amsterdam route

Fig. 3 Examples of demand schedules on routes in the reference network

Table 3 Cost and yield assumptions for the reference network, applicable to all airports or flights

Parameter	**Value**
Remain overnight parking cost (stay cost) [USD/hr]	48
Landing fee [USD/landing]	7.8
Kerosene cost [USD/kg]	0.81 ‡
SAF cost [USD/kg]	1.16 [9]
Liquid hydrogen cost [USD/kg]	4.4 [39]
CO2 tax [USD/kg]	0
Revenue per passenger-kilometer [USD/(pax km)]	0.148

are allocated. These aircraft cover most of the revenue passenger kilometers (65%) by capturing the high demand on domestic routes. Finally, regional aircraft are operated to pick up the remaining profitable demand relatively cheaply and flexibly. However, this aircraft type covers the least amount of RPKs (9%) and contributes only 3% to the overall profit.

Figure 5 presents the routes operated by each aircraft type. The long-range aircraft transfer passengers to transatlantic destinations, except for Dublin, and to high-demand routes to the west coast of the United States of America. The Dublin route is not included in the schedule since it could not be operated profitably considering the assumptions. Although long-range aircraft, in theory, can also operate shorter domestic routes profitably, this option is prevented by the minimum distance constraint discussed below. The medium-range aircraft focuses on domestic routes. This aircraft type is preferred over the other two types since it can operate these routes at a lower cost than the long-range aircraft while being able to carry more passengers than the regional aircraft. Finally, the regional aircraft aims to transport the remaining domestic demand and serve the Central and South American routes, which have a low weekly demand.

Based on this fleet allocation, we conclude that the current dynamic programming approach converges and can realistically model the profit-seeking decision-making process. Nevertheless, we recommend addressing the following

Table 4 Design variables and performance data of kerosene aircraft, partially based on Reference [12]

	REG		SMR		LR	
Variable [Unit]	**COC**	**ATR$_{100}$**	**COC**	**ATR$_{100}$**	**COC**	**ATR$_{100}$**
A [-]	7.95	11.8	7.95	10.9	8.00	12.0
W/S [kN/m^2]	5315	5557	5506	6201	6612	7396
BPR [-]	7.50	9.80	8.17	8.23	10.1	11.0
Π_{fan} [-]	1.80	1.48	1.80	1.48	1.72	1.38
Π_{lpc} [-]	1.48	1.61	1.40	1.72	1.80	1.70
Π_{hpc} [-]	22.4	23.7	23.9	23.3	19.1	25.0
TET [10^3 K]	1516	1481	1548	1443	1605	1454
h_{cr} [km]	9.75	6.00	10.1	6.00	10.8	6.11
M_{cr} [-]	0.78	0.60	0.81	0.60	0.90	0.60
MTOM [-]	35.3	34.2	68.9	65.5	276	264
OEM [-]	20.8	19.8	39.9	36.4	140	127
L/D_{cr} [-]	15.6	16	17.3	17.7	20.4	21.6
TSFC$_{\text{cr}}$ [10^{-5}kg/(N s)]	1.41	1.24	1.42	1.26	1.46	1.2
$\eta_{\text{ov,cr}}$	39%	36%	40%	35%	42%	37%
LTOT	0h19m	0h19m	0h20m	0h20m	0h26m	0h26m
TAT	0h16m	0h16m	0h41m	0h41m	1h26m	1h26m
C_{hour} [10^3 USD/hr]	2.85	2.78	4.19	3.98	10.5	10.4

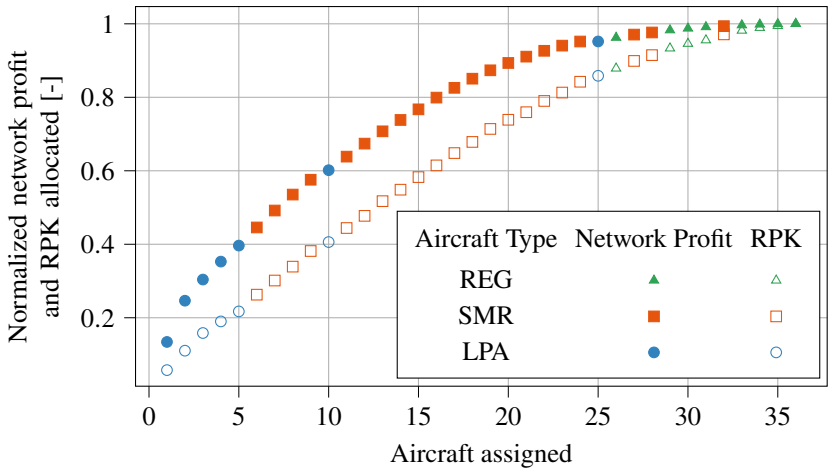

Fig. 4 Convergence of network profit (objective) and allocated RPKs with aircraft allocation. The profit and RPK values are normalized with the total network values.

two characteristics of the current dynamic programming implementation in the future: First, for the considered network, there is a leftover demand from the hub to locations in Europe on the last day of the week and from the same locations in Europe to the hub on the first day of the week. This demand cannot be captured because an aircraft would have to leave at the overseas location on the first day and stay overnight at this location on the last day. However, the current approach imposes that any aircraft should depart from the hub on the first day and end operations at the hub on the last day. The algorithm should be updated to reflect this periodic continuity across the boundaries of the considered period.

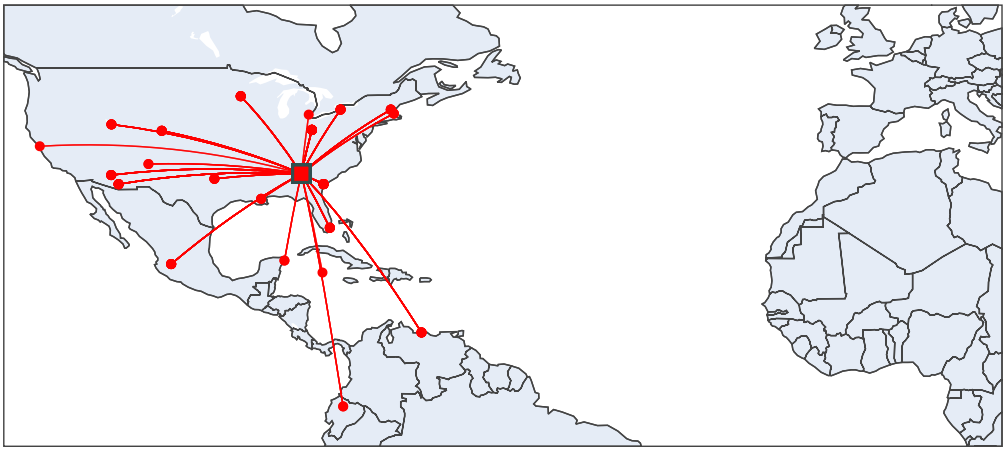

(a) Regional aircraft

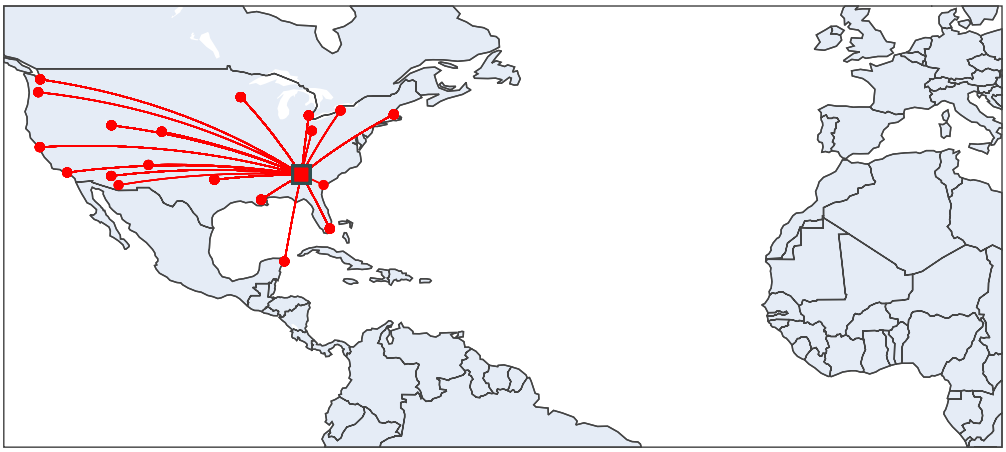

(b) Medium-range aircraft

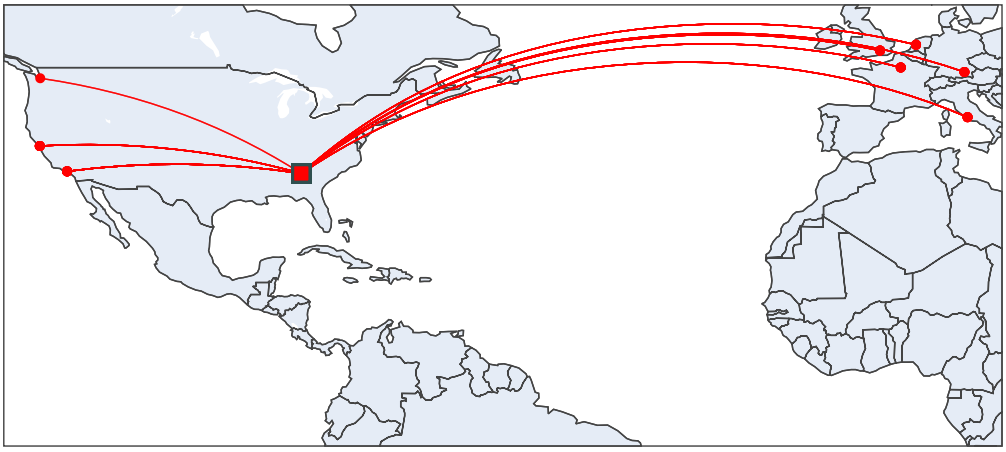

(c) Long-range aircraft

Fig. 5 Routes operated by the three aircraft types considered in the cost-optimal, kerosene case. The square marker indicates the hub (Atlanta International Airport).

Although these missing flights do affect the total revenue and profit, we are mostly interested in the differences between allocating different types of fleets for the same network demand. Hence, all fleets studied in this research experience a similar deficit in uncaptured demand, revenue passenger kilometers, and profit.

Second, when studying the allocation of the cost-optimal aircraft, we observed that the large passenger aircraft were allocated to the transatlantic flights since these routes are the most profitable ones. To fill the weekly schedule of these large passenger aircraft, the algorithm added flights to domestic destinations, which are profitable. Nevertheless, regional or medium-range aircraft may make more profit on these shorter routes since they are less expensive to operate and acquire. But since the demand on these short routes was already partially covered by the large aircraft, the smaller aircraft did not have the chance to transport these passengers in later iterations steps. This led to a sub-optimal allocation of the aircraft. To circumvent this issue, a minimum route distance was imposed on the operations of the large passenger aircraft of 3000 km (1620 nmi). This constraint leads to an increase in overall fleet profit and a reduction in total fuel burn. Although this range is set arbitrarily at the moment, such that only high-demand operations on the West Coast and transatlantic flights can be operated by the large passenger aircraft, it is recommended to choose the constraint value strategically in the future based on relative aircraft operating and ownership costs. Alternatively, longer turn-around times and/or higher operating costs on these routes can penalize domestic operations with the LR type.

IV. Results and Discussion

Using the reference, cost-optimal case introduced in Section III as a starting point, we now employ the method defined in Section II to examine how the aircraft sets designed for a climate objective and powered by different fuels should be allocated to maximize the profit while monitoring the effect on climate impact. First, we only consider the aircraft redesign for the climate objective, using fossil-based kerosene. This is discussed in Section IV.A. Subsequently, the impact of introducing liquid hydrogen- or SAF-powered aircraft concepts is studied in Section IV.B. Throughout this section, the input network demand and the associated demand schedule throughout the week, as described in Section III.A, remain equal, irrespective of the considered design objective or fuel.

A. Allocation of Climate-Optimal, Kerosene-Powered Aircraft

This section studies how climate-optimal, kerosene-powered aircraft should be allocated on the network to maximize profit. These aircraft's design variables and performance metrics are presented in Table 4. Compared to the cost-optimal reference case, a crucial change in the design of these aircraft is the lower cruise altitude to minimize non-CO_2 effects [6]. A reduced cruise Mach number accompanies this lower cruise altitude to maintain a near-optimal lift-to-drag ratio in cruise. However, these changes lead to a lower cruise velocity and a longer mission block time. Therefore, it is hypothesized that these climate-optimal aircraft cannot reach the same productivity level (RPK / unit of time) as the cost-optimal counterparts unless more aircraft of the same capacity are operated.

The changes in fleet composition (i.e., number and types of aircraft) and operations as a result of climate design objective can be found in Tables 5 to 14. The overall network profit is reduced by 21%, while the climate impact decreases by 61%. The reduction in profit is due to the increased operating costs per flight, the reduced cruise speed and longer block time, and the 22% less revenue passenger kilometers covered overall. The latter is expected to be caused by the longer flight time, which limits the consecutive flights per aircraft instance in a given period (day or week).

Similarly, the reason for the reduction in climate impact is twofold. First, the redesigned aircraft feature a lower cruise altitude which targets the contribution due to NO_x emissions and contrail formation. The impact of contrails is eliminated for the climate-optimal kerosene network since the aircraft are flying lower, in conditions where persistent contrails cannot form. Second, we observe a decrease in climate impact due to the reduction in profitable RPKs. This observation is supported by the reduction in energy consumption, and linearly-related CO_2 emissions, in Table 8. At the single-mission level, the CO_2 emissions of the climate-optimal aircraft are equal to or even larger than for the cost-optimal aircraft. Hence, since the emissions are greater or equal at the aircraft level but reduced at the network level, we can deduce that the climate impact is partially reduced because of the decrease in passenger mileage.

In the cost-optimal fleet, the medium-range category contributes most to the climate impact, as shown in Table 7. This corresponds to the highest share of revenue passenger kilometers. When switching to the climate objective, the long-range category becomes relatively more important, while the relative contribution to the network RPKs reduces. We expect that the reason for this is that the maximum achievable climate impact reduction, by changing the design objective, for long-range aircraft is lower than for medium-range aircraft.

To maximize the profit, the climate-optimal fleet requires 41 aircraft, five more than in the case of the cost-optimal fleet. Four medium-range and one long-range aircraft are added to the fleet. In terms of relative profit, RPK, and

departures, we observe the contribution of regional and long-range aircraft to these parameters shifts towards the medium-range category when moving from the cost to the climate objective. Nevertheless, despite the increase in number of SMR aircraft and relative RPK coverage, the number of departures by SMR aircraft stays approximately the same (see Table 13). Although one long-range aircraft is added to the fleet, the total departures among long-range aircraft decrease from 92 to 76, and one destination is removed (Table 14). The weekly flights to Munich (MUC) are stopped since the relatively low demand on this long-range route cannot be captured profitably anymore, while the route to Rome (FCO) with higher demand and similar range is still operated. Similarly, the departures by regional aircraft decreased by 22%, and three designations (Portland, Phoenix, and San Francisco) are no longer operated by regional aircraft.

Previous research indicated that 11, 18, or 36% more aircraft would be required when switching from a cost objective to a climate objective [6], for the regional, medium- and long-range categories, respectively. The current analysis shows that 13% (41 versus 36) more aircraft are allocated, of which none are extra-regional aircraft. This difference exists because of the constant productivity assumption made in previous research, where it was assumed that the same productivity level had to be achieved by the climate-optimal aircraft. However, in this research, we do not impose a constraint on the productivity level or flight frequency but let the profit drive the fleet selection instead. The current analysis shows that the increase in aircraft number is less than previously expected because adding more aircraft would not be profitable. Hence, it would be irrational to acquire 18% or 36% more aircraft if a subset of these cannot be allocated profitably. This aspect makes the current approach more realistic. Additionally, the current approach allows the routes flown and demand captured to vary between objectives and fuels. Nonetheless, the validity of this conclusion is only tested for the reference network considered in this study.

When comparing the average load factor in Table 12, a slight increase in load factor for all aircraft types is present. This indicates that the algorithm tries to have full aircraft, which is now required to ensure that a flight becomes profitable. Nevertheless, the increase in load factor is only marginal since the difference varies between 1 and 4%.

Table 5 Comparison of network profit [Million USD]

		Kerosene	SAF	Hydrogen
Cost	REG	0.7 (3%)	0.6 (3%)	0.4 (3%)
	SMR	12.8 (55%)	10.9 (52%)	12.1 (77%)
	LR	9.9 (42%)	9.3 (45%)	3.2 (20%)
	Total	23.5	20.8	15.7
Climate	REG	0.5 (2%)	0.4 (3%)	0.4 (3%)
	SMR	11.5 (62%)	10.4 (62%)	9.4 (73%)
	LR	6.6 (36%)	6.0 (36%)	3.0 (24%)
	Total	18.6	16.9	12.7

Table 6 Comparison of RPK [10^9 km]

		Kerosene	SAF	Hydrogen
Cost	REG	0.41 (9%)	0.34 (8%)	0.30 (8%)
	SMR	3.01 (65%)	2.81 (64%)	3.12 (78%)
	LR	1.19 (26%)	1.24 (28%)	0.57 (14%)
	Total	4.62	4.39	3.99
Climate	REG	0.27 (8%)	0.25 (7%)	0.22 (7%)
	SMR	2.54 (71%)	2.50 (71%)	2.54 (78%)
	LR	0.79 (22%)	0.77 (22%)	0.48 (15%)
	Total	3.60	3.52	3.25

B. Introduction of Future Aviation Fuels into the Fleet

As discussed in the previous section, redesigning the aircraft for a climate-focused objective such as ATR_{100} can significantly reduce the climate impact of the network by 61%. Nevertheless, introducing future aviation fuels, such as drop-in sustainable aviation fuels and liquid hydrogen, can reduce the climate impact even further, especially when combined with ATR_{100} as the design objective. In this section, we consider aircraft powered by different fuels and how they should be allocated to maximize profit. The aircraft design variables and performance indicators for the LH2- and SAF-powered aircraft sets are summarized in Tables 16 and 17 in Appendix B.

Bringing all design objectives and fuels together results in a total of six case studies. Figure 6a presents the resulting fleet performance of each of these fleets, where the point (1,1) corresponds to the reference cost-optimal, kerosene fleet discussed in Section III. This plot shows that the hydrogen, climate-optimal fleet has the lowest climate impact, but this gain comes at a 46% decrease in the network profit. The large reduction in ATR_{100} is facilitated by the lack of CO_2 emissions and persistent contrails, as well as a reduction in NO_x emission index and reduced radiative forcing due to the lower cruise altitude.

Table 7 Comparison of climate impact [10^{-3} mK]

		Kerosene	SAF	Hydrogen
Cost	REG	12.5 (12%)	6.1 (11%)	3.0 (13%)
	SMR	55.1 (51%)	27.5 (50%)	15.5 (69%)
	LR	40.8 (38%)	21.7 (39%)	3.9 (17%)
	Total	108.5	55.3	22.4
Climate	REG	2.9 (7%)	1.2 (6%)	0.0 (5%)
	SMR	20.6 (48%)	9.4 (47%)	0.4 (55%)
	LR	19.3 (45%)	9.3 (46%)	0.3 (40%)
	Total	42.9	19.9	0.7

Table 8 Comparison of energy consumption [10^{8} MJ]

		Kerosene	SAF	Hydrogen
Cost	REG	0.23 (8%)	0.21 (8%)	0.17 (7%)
	SMR	1.34 (46%)	1.24 (45%)	1.37 (59%)
	LR	1.34 (46%)	1.32 (48%)	0.79 (34%)
	Total	2.91	2.76	2.33
Climate	REG	0.18 (7%)	0.16 (7%)	0.15 (7%)
	SMR	1.29 (51%)	1.26 (51%)	1.40 (63%)
	LR	1.08 (42%)	1.05 (42%)	0.68 (31%)
	Total	2.55	2.47	2.24

Table 9 Comparison of pax transported [10^{3}]

		Kerosene	SAF	Hydrogen
Cost	REG	17 (11%)	14 (10%)	13 (10%)
	SMR	104 (69%)	100 (69%)	109 (80%)
	LR	29 (20%)	32 (22%)	14 (10%)
	Total	150	146	137
Climate	REG	14 (9%)	12 (9%)	10 (8%)
	SMR	105 (73%)	102 (73%)	102 (80%)
	LR	26 (18%)	25 (18%)	15 (12%)
	Total	145	139	127

Table 10 Comparison of distance flown [10^{6} km]

		Kerosene	SAF	Hydrogen
Cost	REG	0.35 (17%)	0.33 (17%)	0.28 (15%)
	SMR	1.19 (57%)	1.11 (57%)	1.28 (69%)
	LR	0.54 (26%)	0.52 (27%)	0.28 (15%)
	Total	2.09	1.96	1.84
Climate	REG	0.28 (15%)	0.25 (14%)	0.24 (15%)
	SMR	1.15 (62%)	1.14 (63%)	1.15 (71%)
	LR	0.43 (23%)	0.42 (23%)	0.23 (14%)
	Total	1.86	1.81	1.62

Table 11 Comparison of number aircraft allocated to the fleet

		Kerosene	SAF	Hydrogen
Cost	REG	8	8	7
	SMR	21	20	23
	LR	7	7	4
	Total	36	35	34
Climate	REG	8	7	6
	SMR	25	25	24
	LR	8	8	4
	Total	41	40	34

Table 12 Comparison of average load factor per flight

		Kerosene	SAF	Hydrogen
Cost	REG	88%	89%	94%
	SMR	91%	91%	95%
	LR	73%	75%	76%
Climate	REG	92%	94%	96%
	SMR	92%	93%	96%
	LR	77%	78%	83%

Between the two extreme solutions, i.e., the kerosene, cost-optimal fleet and the hydrogen, climate-optimal fleet, the SAF-powered counterparts appear to be Pareto optimal. Aircraft using a 50-50 SAF mixture can reduce the climate impact of the fleet between 49 and 82%. The cost-optimal SAF fleet is the closest option to the reference kerosene case. These aircraft are similar in design, except for the small difference in the selected cruise Mach number. Therefore, the reduction in network profit and RPKs is mostly driven by the higher fuel cost of drop-in SAF.

Table 13 Comparison of number of departures

		Kerosene	SAF	Hydrogen
Cost	REG	226 (24%)	192 (21%)	168 (20%)
	SMR	636 (67%)	610 (68%)	642 (75%)
	LR	92 (10%)	96 (11%)	42 (5%)
	Total	954	898	852
Climate	REG	176 (20%)	154 (18%)	128 (17%)
	SMR	634 (72%)	608 (73%)	594 (78%)
	LR	76 (9%)	74 (9%)	40 (5%)
	Total	886	836	762

Table 14 Comparison of number of destinations

		Kerosene	SAF	Hydrogen
Cost	REG	21	20	19
	SMR	19	19	18
	LR	8	8	5
	Total	29	30	26
Climate	REG	18	17	22
	SMR	19	19	18
	LR	7	6	5
	Total	28	28	26

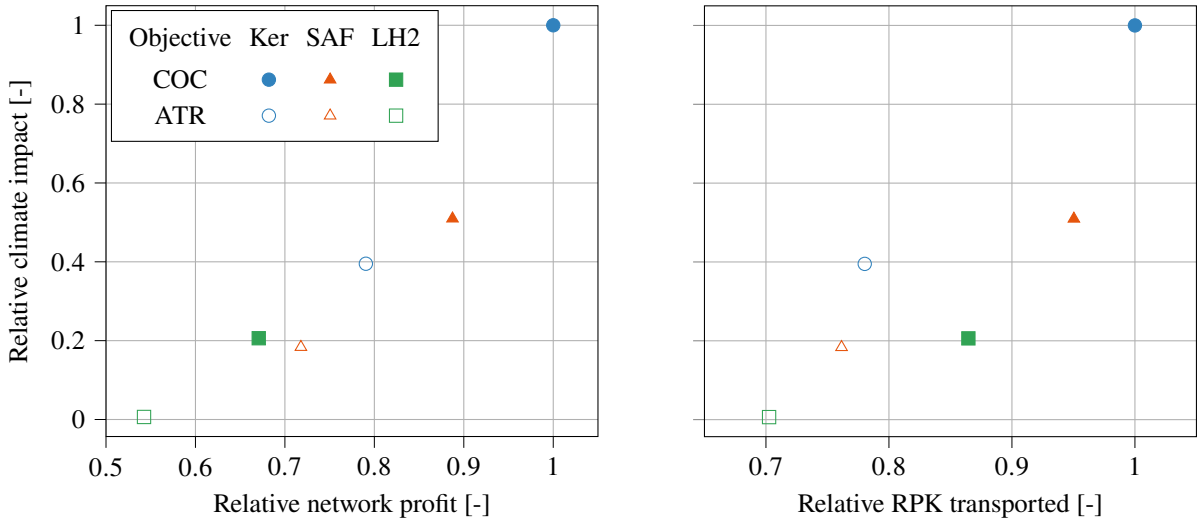

(a) Network profit versus Climate Impact

(b) RPK transported versus Climate Impact

Fig. 6 Comparison between network key performance indicators for different aircraft design objectives and different fuels

In Figure 6b, the revenue passenger kilometers covered by each fleet solution are plotted versus the climate impact. Similar to the observation made in comparing the design objectives in Section IV.A, the SAF- and LH2-powered aircraft reduce the transported RPKs. This results from the different fuel costs and the resulting cruise velocity. SAF and hydrogen have a higher fuel cost per flight since the cost per unit of energy is higher than for kerosene. This makes all flights less profitable. Additionally, the aircraft in the kerosene, cost-optimal fleet are designed to have the highest cruise velocities and shortest block times. The cost-optimized SAF and LH2 aircraft cruise at lower speeds than the kerosene alternative since the fuel-related operating cost becomes relatively more important than the time-bound cost in the design process. Therefore, the LH2 and SAF cost-optimal aircraft designs are closer to an energy-optimal design.

By inspecting the fleet composition and schedule parameters in Tables 9 to 14, we can conclude that the operations do not differ significantly between the kerosene- and SAF-powered fleets. Although the overall amount of passengers transported, flown distance, and number of departures are smaller for the SAF fleet in absolute terms, the relative contribution of each of the three aircraft types is nearly identical to that of the kerosene fleet, for both design objectives. The trends observed in the previous section, such as the increased number of aircraft when the climate objective is selected, also hold for the SAF-powered fleet.

The fleet composition and scheduling choices of the hydrogen aircraft are quite different. The relative contribution of the hydrogen, long-range aircraft to the network profit and RPKs is significantly smaller than for the other two fuels.

Only four long-range aircraft are allocated instead of seven or eight, as shown in Table 11, and only five destinations are operated. Of the set of transatlantic destinations, four are operated, namely Amsterdam, London, Paris, and Rome. The routes to Munich and Dublin are not profitable. Also, the domestic routes to Seattle and San Francisco cannot be operated by hydrogen, long-range aircraft profitably. This difference in operations can also be observed by comparing the allocation shown in Figure 9i to the allocation of the long-range, kerosene counterpart (Figure 9g).

The hydrogen, long-range aircraft, independent of the chosen design objective, is allocated less because of the energy and cost penalties due to the hydrogen tank installation and the higher fuel price. In the current study, this tank is installed aft of the cabin inside the fuselage. The tank itself adds mass to the operating empty mass but also elongates the fuselage. The elongated fuselage structure is heavier and also results in more friction drag. For the considered transatlantic flights, the energy consumption of the hydrogen aircraft is on average 11% higher than for the kerosene alternative, depending on the passenger number and route. Additionally, the hydrogen aircraft cruises at Mach 0.73, instead of 0.88 or 0.90, to have a lower energy consumption. However, this leads to a penalty in mission block time, making it less profitable and making the network allocation more difficult.

The long-range penalties are caused by the long cylindrical tank inside the fuselage. This tank is sized according to the energy and fuel mass needed to match approximately the payload-range capabilities of the Airbus A350-900. However, in this case study, the allocated routes have a shorter range than the design range of a long-range aircraft, as shown in Figure 9i. Therefore, one can conclude that the hydrogen tank is oversized for the routes considered in this network. If we only consider the current network, a logical design decision would be to reduce the design range such that the maximum fuel mass decreases, leading to lower tank volume and a shorter cylindrical tank. This, in turn, reduces the mass and drag penalties at the aircraft level. Potentially, this can also increase the cost-optimal cruise velocity of the aircraft.

Since the loss in overall network profit is mainly caused by the long-range, hydrogen aircraft, the profit figures in Figure 6a are broken down into the three aircraft categories in Figure 7. From these figures, it is clear that the long-range hydrogen aircraft leads to the largest reduction in profit, which cause the overall network profit to decrease. Nevertheless, hydrogen provides a competitive solution in the medium-range category (Figure 7b). In this category, a loss of 5% in profits at a 71% decrease in ATR_{100}, making it a Pareto-optimal solution. Note however that this marginal reduction in network profits is also because now the medium-range aircraft captures a part of the demand to West Coast destinations (LAX, SFO, and SEA) which is captured by long-range aircraft for the kerosene and SAF fleets. For the long-range market, SAF provides Pareto-optimal solutions. The benefit of the cost-optimal SAF aircraft is that its cost-optimal cruise speed is only 2% lower than the kerosene reference aircraft. This minimizes the time penalty which is, in particular, active on long-range flights.

While the payload-range capability of the long-range hydrogen aircraft results in a large tank which makes the aircraft less profitable, the regional hydrogen aircraft appears to have one advantage compared to the kerosene and SAF counterparts. When exchanging payload mass for fuel mass to achieve more range, the hydrogen achieves a larger increase in range for a given reduction in payload mass, compared to the other fuels, due to the high energy density of hydrogen. Therefore, the payload-range diagram features a more gradual slope, as shown in Figure 9c, allowing more payload between 2200 and 3600 km of range. The allocation algorithm makes use of this extra capability and operates flights to Los Angeles, Seattle, and Portland which cannot be captured by the regional kerosene and SAF aircraft.

Table 12 indicates that, when moving from kerosene to SAF and LH2, the average load factors increase marginally. This trend does not necessarily mean that SAF or LH2 aircraft always take more passengers on board than the kerosene alternative. The passenger number on a kerosene flight is also maximized wherever possible due to the equality in Equation (2). This trend in load factor is caused by the fact that kerosene aircraft have a larger profit margin per flight, and can therefore also make profitable flights with fewer passengers on board. When adding flights in the dynamic programming routine throughout the week, the routine can add profitable flights with kerosene without requiring a high load factor. This is for example useful when only little demand is remaining on a given route and there is enough time in the schedule to carry out the flight to add a marginal profit. This leads to a lower average load factor. On the contrary, the higher fuel costs of SAF and LH2 often require a higher load factor before a flight is added to the schedule.

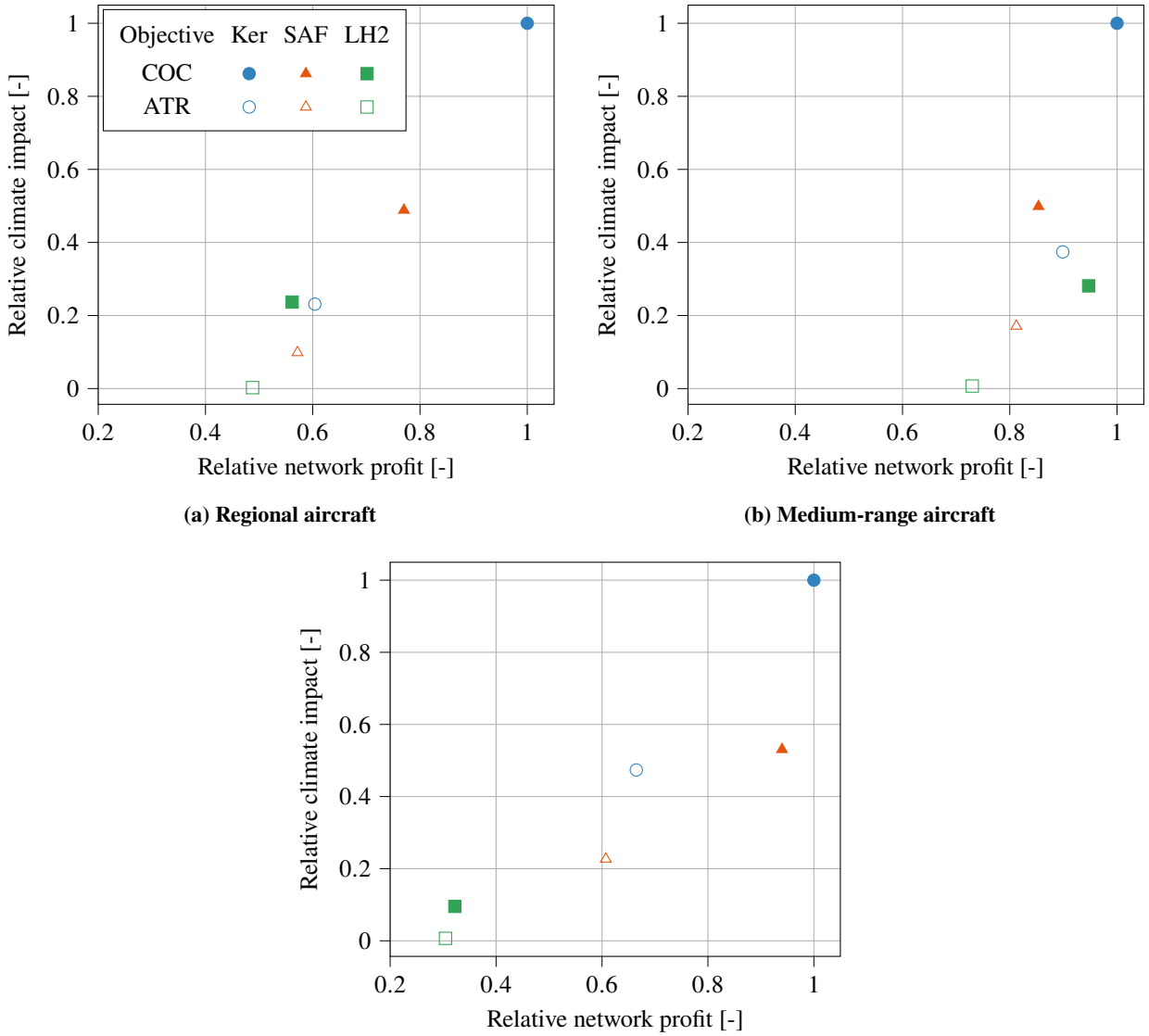

(a) Regional aircraft

(b) Medium-range aircraft

(c) Long-range aircraft

Fig. 7 Comparison between network key performance indicators for different aircraft categories. The values are normalized with the reference metrics of the kerosene, the cost-optimal value for each category.

V. Conclusion

This research aimed to examine how climate-optimal aircraft, considering different fuels, should be allocated on an international network and to monitor the effect on key performance indicators such as total network and climate impact, considering both CO_2 and non-CO_2 effects. We extended a multidisciplinary design analysis and optimization framework to achieve this objective with a fleet allocation and flight scheduling level. This allocation approach employs a dynamic programming routine to find the most profitable allocation of a given set of aircraft types on a US-based network with domestic and international demand. The reference fleet is a set of three cost-optimized, kerosene aircraft targeting different market segments.

We first considered the allocation of climate-optimal, kerosene aircraft, which are characterized by a lower cruise altitude (6 km) and reduced cruise Mach number (0.6). Compared to cost-optimal reference allocation, we observe a 61% reduction in total network ATR_{100}, while the total network profit is reduced by 21%. The reduction in climate impact is caused by a change in aircraft design and a reduction of 22% in revenue passenger kilometers covered. Similarly, the profit reduces because of the lower amount of revenue passenger kilometers operated and an increase in direct flight

operating costs. In particular, the time-related costs increase due to the reduced cruise velocity. The reduced profit margin on flights and lower productivity lead to a lower amount of RPKs covered. We estimate that 41 climate-optimal aircraft are required instead of 36 cost-optimal aircraft.

When aircraft powered by liquid hydrogen or drop-in sustainable aviation fuels are considered, the climate impact can be further reduced. The hydrogen-fueled fleet offers the largest reduction in climate impact up to 99% for the ATR_{100} design objective. However, the network profit is reduced by 45%. We identified that the reason for this is, in particular, the operation of long-range, hydrogen aircraft, which suffer from a significant penalty in operating costs and flight time. The long-range, hydrogen aircraft covers up to 51% less RPKs than its kerosene counterpart. This highlights the need for aircraft solutions for tailored payload-range capabilities. Nevertheless, the medium-range, hydrogen aircraft offer more competitive solutions with a climate impact reduction between 72 and 99%, while only reducing the profit of mid-range operations between 5 and 27%. The fleets fueled by drop-in SAF offer Pareto-optimal solutions. Overall, this analysis highlights that the current coupled approach between aircraft design and network operations can yield useful insights regarding the profitability and composition of climate-optimal fleets.

The conclusions drawn in this study are specific to the type of network considered. We did not consider transfer passengers or the demand between destination airports. Additionally, a fixed demand schedule and constant attraction bands were assumed. Therefore, a first recommendation is to conduct a sensitivity analysis to establish the sensitivity of the results and conclusions to these assumptions. Secondly, the current study analyzes the allocation of optimized aircraft in a network but does not yet feed the information back to the aircraft design loop. Hence, we recommend establishing this link to determine the optimal payload-range requirements and possibly a design objective function that combines the cost and climate impact metrics.

Appendix

A. Top-level Aircraft Requirements

This appendix introduces the TLARs used in the fleet design.

Table 15 Top-level aircraft requirements employed for the aircraft design [12, 40–42] in the benchmark case

Requirement [Unit]	Regional	Medium-Range	Long-Range
Maximum structural payload $m_{\text{pl,max}}$ [metric tons]	10.1	18.2	54.0
Harmonic range r_{harm} [km (nm)]	2410 (1300)	3200 (1730)	10800 (5830)
Ferry range r_{ferry} [km (nm)]	4630 (2500)	6750 (3645)	18000 (9720)
Approach speed v_{app} [m/s (kts)]	69.0 (134)	70.0 (136)	72.0 (140)
Take-off length (ISA conditions) [m (ft)]	1700 (5580)	2100 (6890)	2700 (8860)
ICAO Reference Code	3C	4C	4E
Maximum span b_{max} [m]	36.0	36.0	65.0
Diversion range r_{div} [km (nm)]	185 (100)	463 (250)	463 (250)
Loiter time t_{hold} [min]	45	35	35
Landing mass factor f_{W} kerosene and SAF [-]	0.91	0.88	0.73
Landing mass factor f_{W} hydrogen [-]	0.97	0.94	0.87
Mass of operational items m_{ops} [t]	2.42	4.77	15.4
Mass of airframe systems and equipment m_{afse} [t]	4.46	8.81	22.5

B. Demand and Allocation of Reference Network

Figures 8a and 8b present the initial and final, remaining demand of the reference network case, employing cost-optimal, kerosene aircraft. In Figure 9, the allocation of the different cost-optimized, kerosene and hydrogen aircraft is shown.

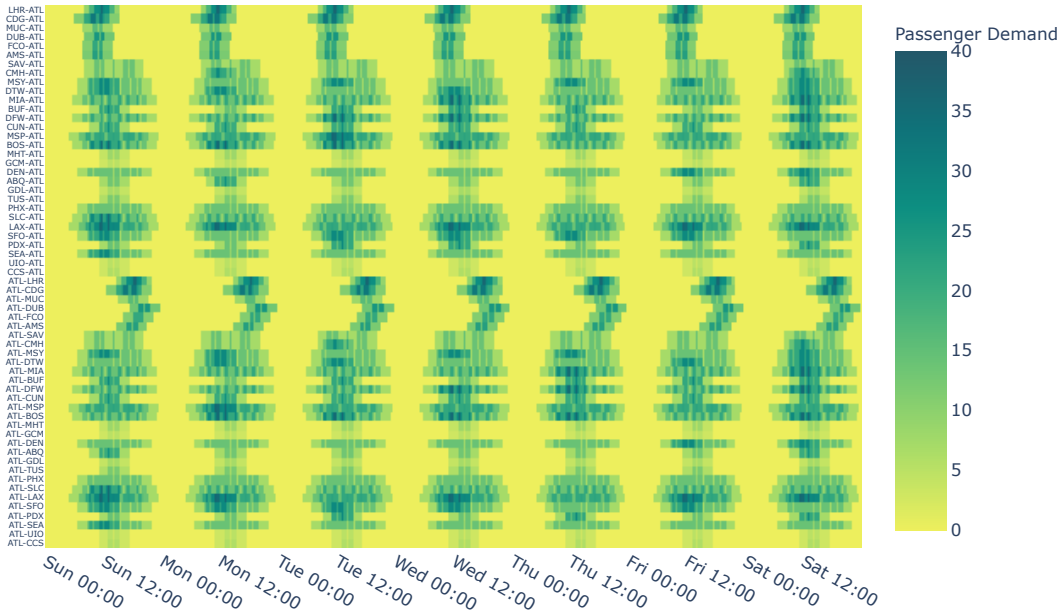

(a) Initial demand schedule (input)

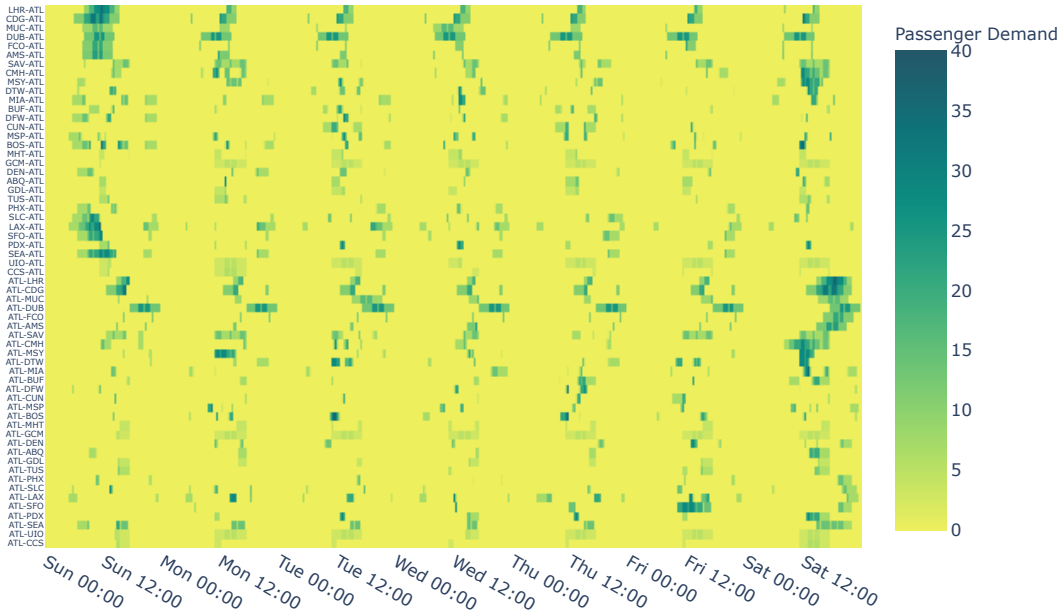

(b) Final remaining demand (after iterations converged)

Fig. 8 Passenger demand schedules between origin-destination pairs (y-axis) at all 20-minute time intervals (x-axis) throughout one week

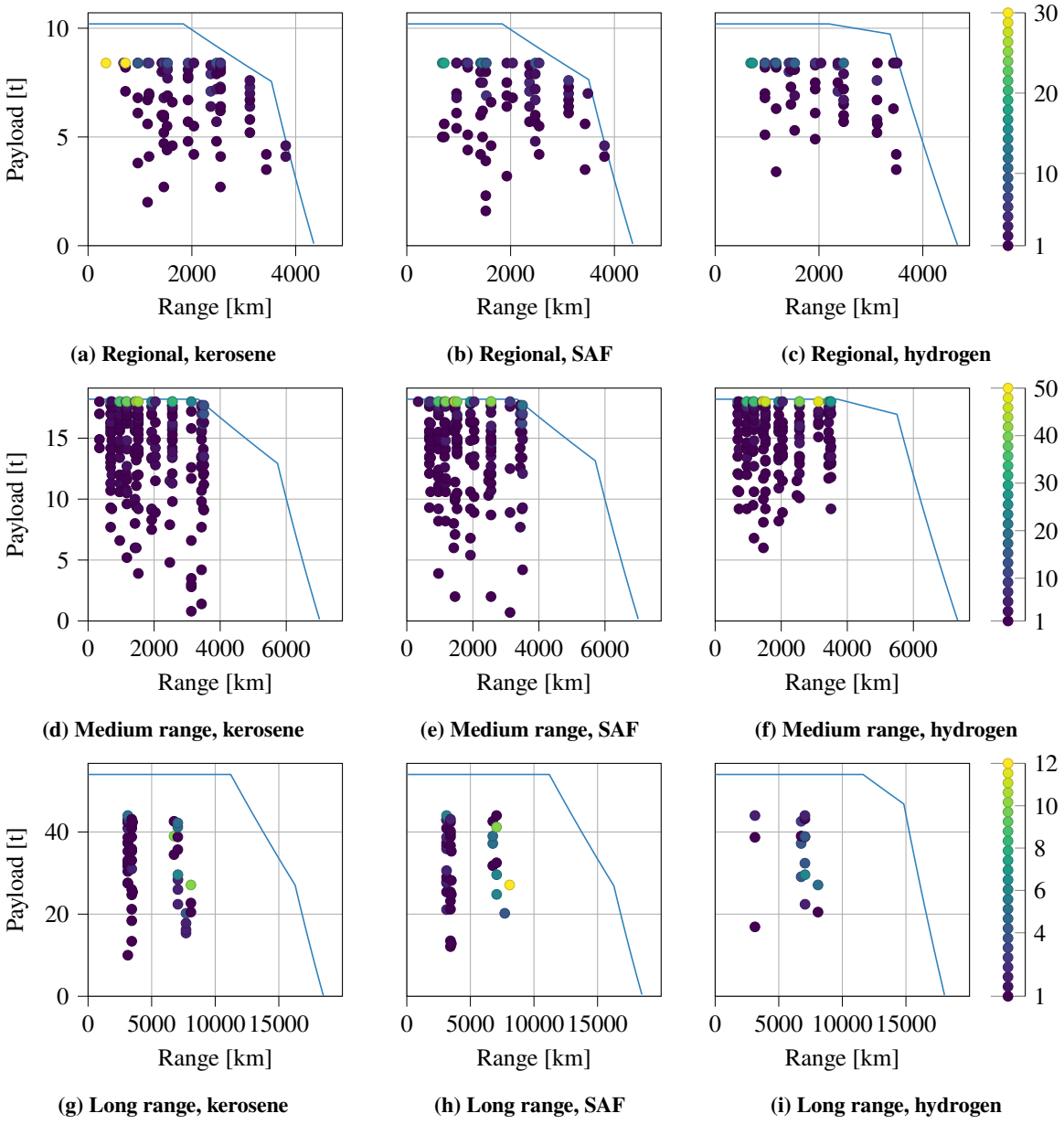

(a) Regional, kerosene (b) Regional, SAF (c) Regional, hydrogen

(d) Medium range, kerosene (e) Medium range, SAF (f) Medium range, hydrogen

(g) Long range, kerosene (h) Long range, SAF (i) Long range, hydrogen

Fig. 9 Payload-range diagram and operated payload-range combinations for each aircraft type. The colorbar indicates the flight frequency of a payload-range combination in one week.

C. Design Data of Aircraft Powered by Liquid Hydrogen or SAF

This appendix presents the aircraft design data of the fleets powered by liquid hydrogen or drop-in SAF.

Table 16 Design variables and performance data of liquid-hydrogen aircraft, partially based on Reference [12]

	REG		SMR		LR	
Variable [Unit]	**COC**	**ATR$_{100}$**	**COC**	**ATR$_{100}$**	**COC**	**ATR$_{100}$**
A [-]	12.0	10.9	11.4	11.1	11.1	12.0
W/S [kN/m^2]	5329	5545	5570	5310	6391	6780
BPR [-]	8.00	9.35	9.57	8.33	11.0	11.0
Π_{fan} [-]	1.80	1.59	1.76	1.55	1.65	1.47
Π_{lpc} [-]	1.68	1.79	1.37	1.56	1.66	1.76
Π_{hpc} [-]	19.8	21.1	25.0	24.6	21.9	23.1
TET [10^3 K]	1450	1504	1520	1450	1556	1484
h_{cr} [km]	10.4	6.00	10.4	6.00	9.35	6.00
M_{cr} [-]	0.71	0.60	0.73	0.60	0.73	0.60
MTOM [t]	33.1	32.2	64.5	63.6	248	244
OEM [t]	21.5	20.5	42.6	41.2	163	156
L/D_{cr} [-]	17.4	15	18.5	16.5	20.4	19.7
TSFC$_{\text{cr}}$ [10^{-5}kg/(N s)]	0.468	0.445	0.468	0.451	0.465	0.43
$\eta_{\text{ov,cr}}$	38%	36%	39%	35%	40%	37%
LTOT	0h19m	0h19m	0h20m	0h20m	0h25m	0h26m
TAT	0h16m	0h16m	0h41m	0h41m	1h26m	1h26m
C_{hour} [10^3 USD/hr]	2.85	2.79	4.31	4.17	11.4	11.5

Table 17 Design variables and performance data of SAF aircraft [12], partially based on Reference [12]

	REG		SMR		LR	
Variable [Unit]	**COC**	**ATR$_{100}$**	**COC**	**ATR$_{100}$**	**COC**	**ATR$_{100}$**
A [-]	8.31	11.4	8.58	11.9	8.00	12.0
W/S [kN/m^2]	5431	5637	5620	6030	6652	7646
BPR [-]	5.89	8.45	8.04	8.72	8.82	11.0
Π_{fan} [-]	1.80	1.53	1.80	1.43	1.65	1.37
Π_{lpc} [-]	1.33	1.56	1.58	1.67	1.27	1.62
Π_{hpc} [-]	25.0	25.0	20.9	25.0	23.0	25.0
TET [10^3 K]	1425	1489	1540	1420	1459	1436
h_{cr} [km]	9.77	6.00	9.95	6.00	10.4	6.00
M_{cr} [-]	0.77	0.60	0.79	0.60	0.88	0.60
MTOM [t]	34.7	33.8	68.1	66	275	262
OEM [t]	20.3	19.4	39.3	37.1	138	126
L/D_{cr} [-]	15.8	15.9	17.7	18	20.3	21.4
TSFC$_{\text{cr}}$ [10^{-5}kg/(N s)]	1.41	1.25	1.39	1.23	1.45	1.2
$\eta_{\text{ov,cr}}$	38%	35%	39%	35%	41%	36%
LTOT	0h19m	0h19m	0h20m	0h20m	0h26m	0h26m
TAT	0h16m	0h16m	0h41m	0h41m	1h26m	1h26m
C_{hour} [10^3 USD/hr]	2.83	2.75	4.22	4.05	10.3	10.3

Acknowledgments

This research is partially funded by the European Union's Clean Sky 2 Thematic Topics program (H2020-EU.3.4.5.10.) with grant agreement numbers 865300 (GLOWOPT project) and 101007715 (CHYLA project). Special thanks to dr. ir. Maurice Hoogreef for bringing aircraft design and operations closer together. The dynamic programming approach in this paper is based on the work in the MSc. Thesis of María Seaone Álvarez.

References

[1] Stan, S., and Bob, L., *Global Market Forecast 2022*, Airbus S.A.S., 2022.

[2] Boeing, *Commercial Market Outlook 2022-2041*, Boeing, 2022.

[3] Antoine, N. E., and Kroo, I. M., "Framework for Aircraft Conceptual Design and Environmental Performance Studies," *AIAA Journal*, Vol. 43, No. 10, 2005, pp. 2100–2109. https://doi.org/10.2514/1.13017.

[4] Schwartz Dallara, E., Kroo, I. M., and Waitz, I. A., "Metric for Comparing Lifetime Average Climate Impact of Aircraft," *AIAA Journal*, Vol. 49, No. 8, 2011, pp. 1600–1613. https://doi.org/10.2514/1.J050763.

[5] Dahlmann, K., Koch, A., Linke, F., Lührs, B., Volker, G., Otten, T., Seider, D., Gollnick, V., and Schumann, U., "Climate-Compatible Air Transport System—Climate Impact Mitigation Potential for Actual and Future Aircraft," *Aerospace*, Vol. 3, 2016, p. 38. https://doi.org/10.3390/aerospace3040038.

[6] Proesmans, P., and Vos, R., "Airplane Design Optimization for Minimal Global Warming Impact," *Journal of Aircraft*, Vol. 59, No. 5, 2022, pp. 1363–1381. https://doi.org/10.2514/1.C036529.

[7] Contreras, A., Yiğit, S., Özay, K., and Veziroğlu, T., "Hydrogen as aviation fuel: a comparison with hydrocarbon fuels," *International Journal of Hydrogen Energy*, Vol. 22, No. 10-11, 1997, pp. 1053–1060.

[8] de Jong, S., Antonissen, K., Hoefnagels, R., Lonza, L., Wang, M., Faaij, A., and Junginger, M., "Life-cycle analysis of greenhouse gas emissions from renewable jet fuel production," *Biotechnology for Biofuels*, Vol. 10, No. 64, 2017. https://doi.org/10.1186/s13068-017-0739-7.

[9] World Economic Forum, "Clean Skies for Tomorrow - Sustainable Aviation Fuels as a Pathway to Net-Zero Aviation," Tech. rep., Nov 2020.

[10] Burkhardt, U., Bock, L., and Bier, A., "Mitigating the contrail cirrus climate impact by reducing aircraft soot number emissions," *npj Climate and Atmospheric Science*, Vol. 1, No. 1, 2018, p. 37. https://doi.org/10.1038/s41612-018-0046-4.

[11] Moore, R. H., Thornhill, K. L., Weinzierl, B., Sauer, D., D'Ascoli, E., Kim, J., Lichtenstern, M., Scheibe, M., Beaton, B., Beyersdorf, A. J., Barrick, J., Bulzan, D., Corr, C. A., Crosbie, E., Jurkat, T., Martin, R., Riddick, D., Shook, M., Slover, G., Voigt, C., White, R., Winstead, E., Yasky, R., Ziemba, L. D., Brown, A., Schlager, H., and Anderson, B. E., "Biofuel blending reduces particle emissions from aircraft engines at cruise conditions," *Nature*, Vol. 543, No. 7645, 2017, pp. 411–415. https://doi.org/10.1038/nature21420.

[12] Proesmans, P., and Vos, R., "Comparison of Future Aviation Fuels to Minimize the Climate Impact of Commercial Aircraft," *AIAA Aviation 2022 Forum*, Chicago, IL and Virtual, 2022. https://doi.org/10.2514/6.2022-3288.

[13] Gangoli Rao, A., Yin, F., and Werij, H., "Energy Transition in Aviation: The Role of Cryogenic Fuels," *Aerospace*, Vol. 7, 2020, p. 181. https://doi.org/10.3390/aerospace7120181.

[14] Khandelwal, B., Karakurt, A., Sekaran, P. R., Sethi, V., and Singh, R., "Hydrogen powered aircraft : The future of air transport," *Progress in Aerospace Sciences*, Vol. 60, 2013, pp. 45–59. https://doi.org/10.1016/j.paerosci.2012.12.002.

[15] Verstraete, D., Hendrick, P., Pilidis, P., and Ramsden, K., "Hydrogen fuel tanks for subsonic transport aircraft," *International Journal of Hydrogen Energy*, Vol. 35, No. 20, 2010, pp. 11085–11098. https://doi.org/10.1016/j.ijhydene.2010.06.060.

[16] Jansen, P. W., and Perez, R. E., "Robust Coupled Optimization of Aircraft Design and Fleet Allocation for Multiple Markets," *AIAA/3AF Aircraft Noise and Emissions Reduction Symposium*, Atlanta, GA, 2014. https://doi.org/10.2514/6.2014-2735.

[17] Jansen, P. W., and Perez, R. E., "Coupled Optimization of Aircraft Families and Fleet Allocation for Multiple Markets," *Journal of Aircraft*, Vol. 53, No. 5, 2016, pp. 1485–1504. https://doi.org/10.2514/1.C033646.

[18] Perez, R. E., and Jansen, P. W., "Coupled aircraft design and staging assignment for long–range operations," *Journal of Aerospace Operations*, Vol. 4, No. 4, 2017, pp. 223–243. https://doi.org/10.3233/AOP-170064.

[19] Moolchandani, K., Govindaraju, P., Roy, S., Crossley, W. A., and DeLaurentis, D. A., "Assessing Effects of Aircraft and Fuel Technology Advancement on Select Aviation Environmental Impacts," *Journal of Aircraft*, Vol. 54, No. 3, 2017, pp. 857–869. https://doi.org/10.2514/1.C033861.

[20] Hwang, J., Roy, S., Kao, J., Martins, J. R. R. A., and Crossley, W. A., "Simultaneous aircraft allocation and mission optimization using a modular adjoint approach," *56th AIAA/ASCE/AHS/ASC Structures, Structural Dynamics, and Materials Conference*, 2015. https://doi.org/10.2514/6.2015-0900.

[21] Bernardo, J. E., Zaidi, T., LeVine, M., Jimenez, H., and Mavris, D., "Rapid Integrated Interdependent Fleet-Level Environmental Model," *Journal of Aircraft*, Vol. 54, No. 3, 2017, pp. 939–954. https://doi.org/10.2514/1.C033572.

[22] Govindaraju, P., Davendralingam, N., and Crossley, W. A., "A Concurrent Aircraft Design and Fleet Assignment Approach to Mitigate Environmental Impact through Fuel Burn Reduction under Operational Uncertainty," *Journal of Aerospace Operations*, Vol. 4, No. 4, 2017, pp. 163–184. https://doi.org/10.3233/AOP-170061.

[23] Obert, E., *Aerodynamic Design of Transport Aircraft*, IOS press, 2009.

[24] Torenbeek, E., *Synthesis of Subsonic Airplane Design*, Delft University Press and Kluwer Academic Publishers, Dordrecht, 1982.

[25] Mattingly, J. D., Heiser, W. H., and Pratt, D. T., *Aircraft Engine Design*, 2nd ed., American Institute of Aeronautics and Astronautics (AIAA), 2002. https://doi.org/10.2514/4.861444.

[26] Walsh, P. P., and Fletcher, P., *Gas turbine performance*, 2nd ed., Blackwell Science Ltd, Oxford, 2004.

[27] Proesmans, P., and Vos, R., "Hydrogen, Medium-Range Airplane Design Optimization for Minimal Global Warming Impact," *Aerospace Europe Conference 2021*, The Council of European Aerospace Societies (CEAS), Warsaw, 2021.

[28] Torenbeek, E., "The initial calculation of range and mission fuel during conceptual design," Tech. Rep. LR-525, Delft University of Technology, Faculty of Aerospace Engineering, 1987.

[29] Ruijgrok, G. J., *Elements of airplane performance*, VSSD, 2009.

[30] Seaone Álvarez, M., "Assessment of Climate Impact Mitigation Potential of Intermediate Stop Operations," Msc, Delft University of Technology, Delft, Aug 2021.

[31] Noorafza, M., Santos, B., Sharpanskykh, A., Zengerling, Z., Weder, C., Linke, F., and Grewe, V., "Airline Network Planning Considering Climate Impact: Assessing New Operational Improvements," *Applied Sciences, under review*, 2023.

[32] Bellman, R., "On a routing problem," *Quarterly of applied mathematics*, Vol. 16, No. 1, 1958, pp. 87–90.

[33] Ford Jr, L. R., "Network flow theory," Tech. Rep. P-923, Rand Corp Santa Monica Ca, 1956.

[34] Roskam, J., *Airplane Design. Part VIII: Airplane Cost Estimation: Design, Development, Manufacturing and Operating*, DARcorporation, 1985.

[35] Proesmans, P., and Vos, R., "Airplane Design Optimization for Minimal Global Warming Impact," *AIAA Scitech 2021 Forum*, American Institute of Aeronautics and Astronautics (AIAA), Virtual event, 2021, p. 1297. https://doi.org/10.2514/6.2021-1297.

[36] Koch, A., "Climate Impact Mitigation Potential given by Flight Profile and Aircraft Optimization," Phd, Technischen Universität Hamburg-Harburg, Hamburg, Germany, Nov 2013. https://doi.org/10.13140/RG.2.1.4896.9047.

[37] Burkhardt, U., and Kärcher, B., "Global radiative forcing from contrail cirrus," *Nature climate change*, Vol. 1, No. 1, 2011, pp. 54–58.

[38] Jansen, P. W., and Perez, R. E., *Coupled Optimization of Aircraft Design and Fleet Allocation with Uncertain Passenger Demand*, 2013, pp. 2013–4392. https://doi.org/10.2514/6.2013-4392.

[39] Hydrogen Council, "Path to hydrogen competitiveness: A cost perspective," Tech. rep., Jan 2020.

[40] Embraer S.A, "Embraer 175 Airport Planning Manual," Tech. rep., Embraer S.A, 2021.

[41] Airbus S.A.S. Customer Services, "Airbus A320 Aircraft Characteristics Airport and Maintenance Planning," Tech. rep., Airbus S.A.S. Customer Services, 2019.

[42] Airbus S.A.S. Customer Services, "Airbus A350 Aircraft Characteristics Airport and Maintenance Planning," Tech. rep., Airbus S.A.S. Customer Services, 2020.